Spring 2019

Unified probe launch pattern design and methodology of differential probe characterization

Han Deng

Department:

UNIFIED PROBE LAUNCH PATTERN DESIGN AND METHODOLOGY OF DIFFERENTIAL PROBE CHARACTERIZATION

by

HAN DENG

A THESIS

Presented to the Faculty of the Graduate School of the

MISSOURI UNIVERSITY OF SCIENCE AND TECHNOLOGY

In Partial Fulfillment of the Requirements for the Degree

MASTER OF SCIENCE IN ELECTRICAL ENGINEERING

2019

Approved by:

Dr. James. L. Drewniak, Advisor
Dr. Jun Fan
Dr. Chulsoon Hwang
Dr. Qinghua Chen

ABSTRACT

Differential probe is wildly used in the signal integrity area to do the accuracy signal measurement in frequency domain or time domain. Comparing with traditional SMA connector measurement, the probe measurement has several advantages such as the high flexibility and measurement efficiency. Nevertheless, the probe has some disadvantages such as multiple design patterns and the difficulty of fast landing. In this thesis, a unified probe landing pattern is provided to solve the con of probes and a probe testing fixture is designed for characterize probe and extract the probe model.

In the first portion, a unified differential probe launching pattern is proposed for universal usage of different types of differential probes. Full wave-modeling of the transition with the unified probe launching pattern is developed for optimization of dimensions. For the unified probe launching pattern evaluation, 16-layer test vehicles were designed with engineered transitions for performance up to 40 GHz. Four-port measurement results of different differential pairs from the test vehicle are used as the 2x thru reference and DUT for de-embedding. By using GSSG probe, accurate DK and DF along with frequency can be extracted.

In the second portion, a probe testing fixture is designed based on the unified probe launch pattern design to characterize the performance of probe based on the smart fixture de-embedding method. The full wave model is extracted from the fixture design to server future probing measurement design and the circuit model is extracted to study the effectiveness from the specific portion behavior.

ACKNOWLEDGMENTS

First of all, I would like to express my sincere gratitude to my advisor, Dr. James. L. Drewniak, for his support and guidance during my whole master program. His invaluable advice and constant encouragement helped me overcome many difficulties. Then, I also want to thank Dr. Jun Fan, Dr. Chulsoon Hwang and Dr. Qinghua Chen for helping in my research.

I also want to thank my parents for encouraging and supporting me to continue studying, no matter if the results are good or bad. Additionally, I want to thank all members from the Electromagnetic Compatibility Laboratory of Missouri University of Science and Technology. Without their help, I could not have finished my research smoothly.

TABLE OF CONTENTS

Page

LIST OF ILLUSTRATIONS

Page

LIST OF TABLES

Page

1. INTRODUCTION

Micro-probes [20-21] are increasingly more ubiquitous in high-frequency measurements for characterization of accuracy differential signal measurement. Most commercial differential probes need a unique probe launching footprint, though the dimensions of different launching patterns are very similar. Therefore, to improve the efficiency and accuracy of probe measurements, a unified probe launching pattern is proposed to fit most commercial RF probes. A test vehicle with the unified probe launching pad is designed for a differential signal measurement and print circuit board material extraction.

In this paper, two kinds of pitch size unified probe launch patterns are studied, i.e., 1 mm and 0.5 mm pitch. For the both pitch sizes of the unified probe launch patterns, full wave models of the launching pattern are developed for several kinds of probe model [1-3], Signal-Signal (SS) probe, Signal-Ground-Signal (GSG) probe, and, Ground-Signal-Signal-Ground (GSSG) probe [5]. All of the probes are landed on the unified probe launch pattern to get the insertion loss of the differential pairs.

For further probe measurements and the unified probe launching pattern evaluation, two test vehicles with the two pitch sizes of unified probe launching pattern are designed. Both of the designed test vehicles are 16-layer boards with differential pairs located in Layer 1, Layer 10, Layer 12 and Layer 14 with three different lengths on each layer of 2 inches, 5 inches and 10 inches. To ensure good quality of the fixture for de-embedding [4], a full wave model is developed to optimize the transition [10], which includes the studied probe, the unified launching pattern and the differential pairs. For the

0.5mm pitch unified probe launch pattern, the final optimized transition has adequate performance up to 40 GHz. The probe landing is studied based on the 0.5 mm pitch unified probe launch pattern full wave model.

The test vehicle with 1mm pitch unified probe launch pattern is manufactured and measured for the system characterization and material extraction. Four-port measurement results of the different pairs are used as the 2x thru reference and DUT respectively for de-embedding [7-9]. Then the results after de-embedding are used for extracting the DK and DF [6-7] of the board. The test vehicle with 0.5 mm pitch unified probe launch pattern is designed to add 2.92 mm connector measurement section as a golden standard to verify the probe measurement results.

2. UNIFIED PROBE LAUNCH PATTERN – 1MM PITCH

In this section, the 1mm pitch unified probe launch pattern design is detailed in four portions, the probe launch pattern design, the full wave model of the unified probe launch pattern transition optimization, the test vehicle with the unified probe launch pattern design and measurement, and, the printed circuit board DK and DF extraction.

2.1. UNIFIED PROBE LAUNCH PATTERN DESIGN

Due to more and more microprobes being used in the RF measurement, a unified probe launch pattern is advantageous for accommodating different commercial microprobes. For increasing the utility of the differential probe launch pattern, three different 1 mm probe pitch launch patterns are studied as shown in Figure 2.1.

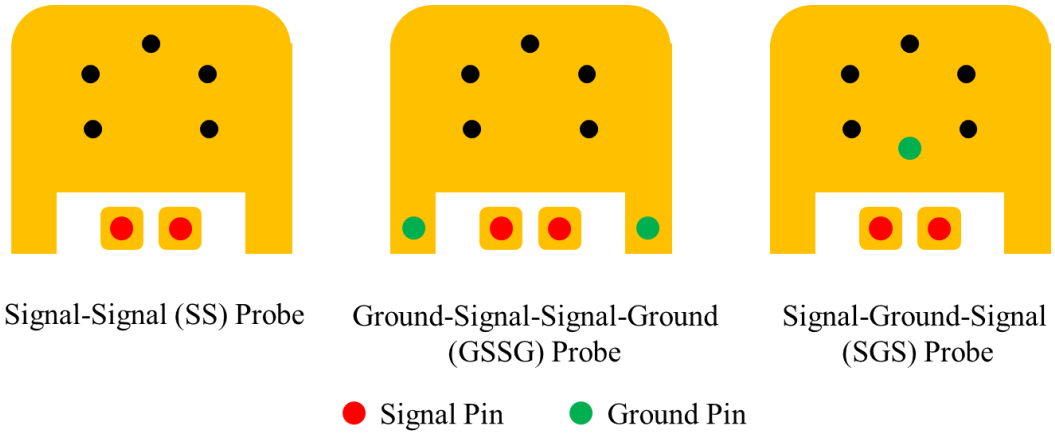

Figure 2.1. Differential probe launch patterns.

From the Figure 2.1, three basic probe designs are considered, i.e., signal-signal (SS) probe, signal-ground-signal (SGS) probe and ground-signal-signal-ground (GSSG)

probe. For each probe design, the pitch size of signal pins is the same 1 mm, and the difference of the three probe launch patterns is the ground pin landing location. Considering whether the probe has the ground pin and the position of the ground pin, a U-shape ground is provided for guaranteeing that any ground pin landing is well accommodated.

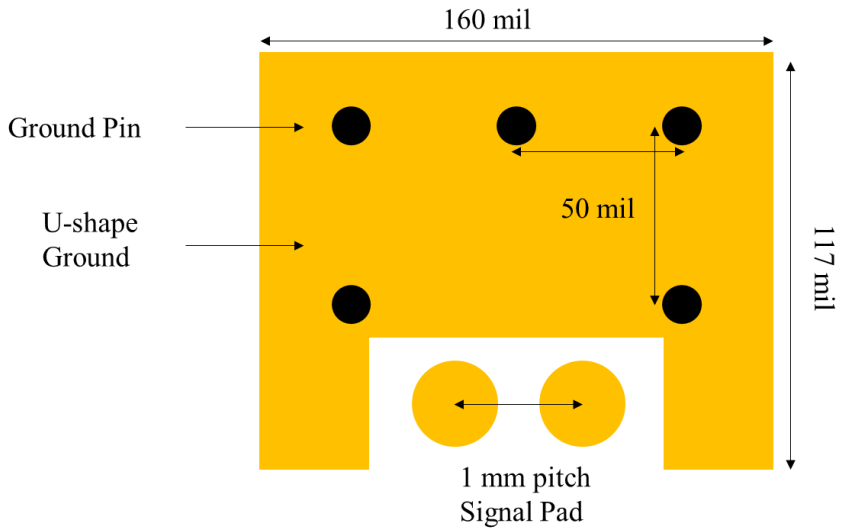

Figure 2.2. 1 mm pitch unified probe launch pattern dimensions.

In the unified probe launch pattern, Figure 2.2, a 160 mil x 117 mil U-shape ground area is added around the differential signal pins. A pair of signal pads has 1mm pitch at the bottom of the U-shape ground plane. Five ground vias are on the U-shape for providing a good landing and connection to the reference for the ground pins.

2.2. FULL WAVE TRANSITION MODEL DESIGN

Full wave modeling of the transition is undertaken for the unified probe launch pattern, which consists of three parts, a differential probe whose differential impedance is 100 Ω, the unified probe launch pattern, and a pair of differential traces, whose differential impedance is 85 Ω. Due to the impedance mismatch between the probe and the differential pairs, the impedance transition geometry design and optimization is very important.

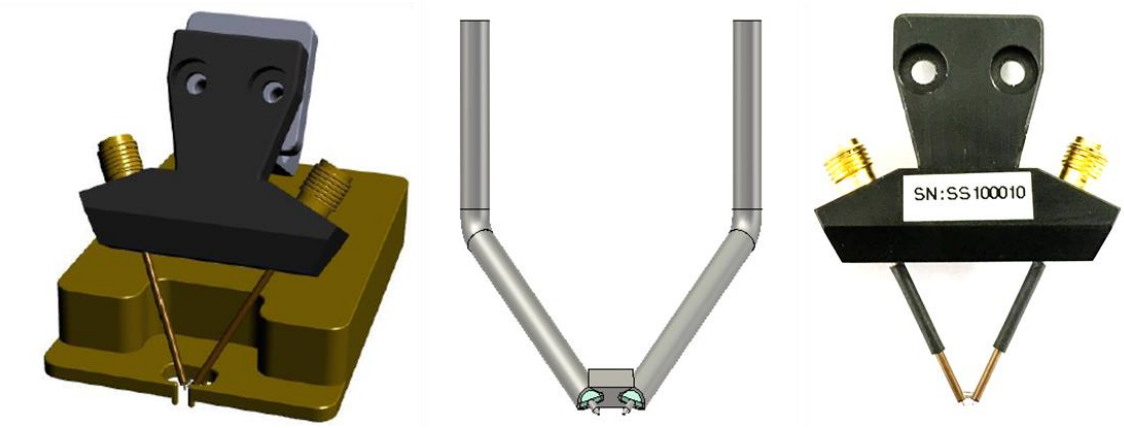

(a) (b) (c)

Figure 2.3. (a) Differential probe with mechanical holder 3D model, (b) simplified full wave differential probe model, (c) manufactured differential probe.

A signal-signal (SS) differential probe is designed and manufactured, which provides high accuracy and efficiency in simulation and measurement. In Figure 2.3(a), a 3D model is used to show the complete probe geometry and a metal base with guide-pins is used to ensure a repeatable probe landing. For the full wave simulation, a simplified probe model is provided based on the complete 3D model as shown in Figure 2.3(b). In

the simplified full wave probe model, the mechanical base portion is removed to reduce the complexity of the model and save the simulation time. In Figure 2.3(c), according to the probe model design, the signal-signal (SS) differential model is manufactured and used for the 4-port S-parameter measurements.

In addition to the new differential probe model, the full wave transition model is developed as shown in Figure 2.4. In this model, the transition part works on the 16 layer boards, and the new differential probe lands on the unified probe launch pattern. The signal is transmitted from the launch pattern through the microstrip and differential vias to the differential stripline at Layer 10, which is the worst case with the longest via stub.

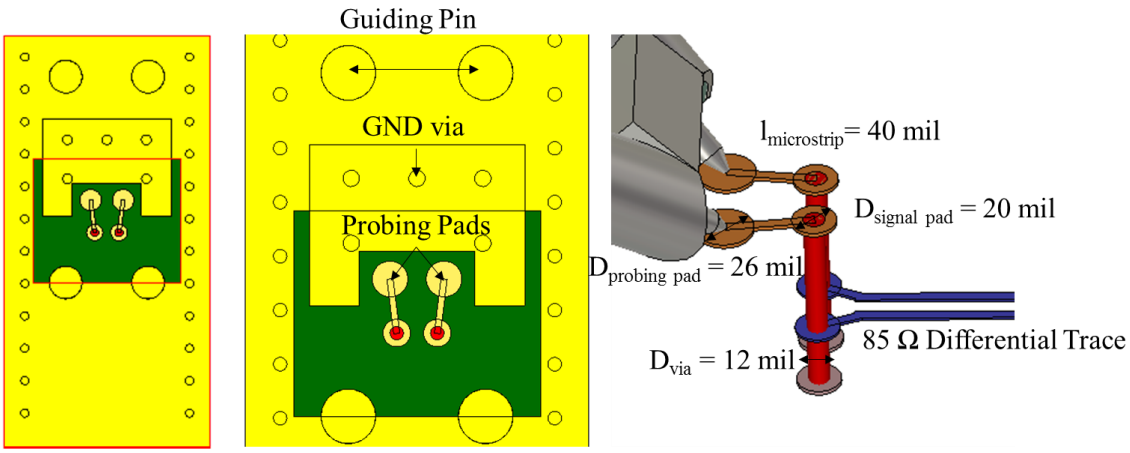

Figure 2.4. (a) Top view of the full wave impedance transition model, (b) the detailed view of the unified launch pattern, and (c) the side view of the transition model.

The goal of the simulation optimization is to make the impedance transition sufficiently smooth to allow for de-embedding [18]. After several iterations of the geometry of the transition, the best simulation results are shown in Figure 2.5. From the

$|S_{dd11}|$ result, the return loss of the transition model is around the 15 dB up to 20 GHz, and the insertion loss, less than 1 dB at 20GHz, as seen from $|S_{dd21}|$.

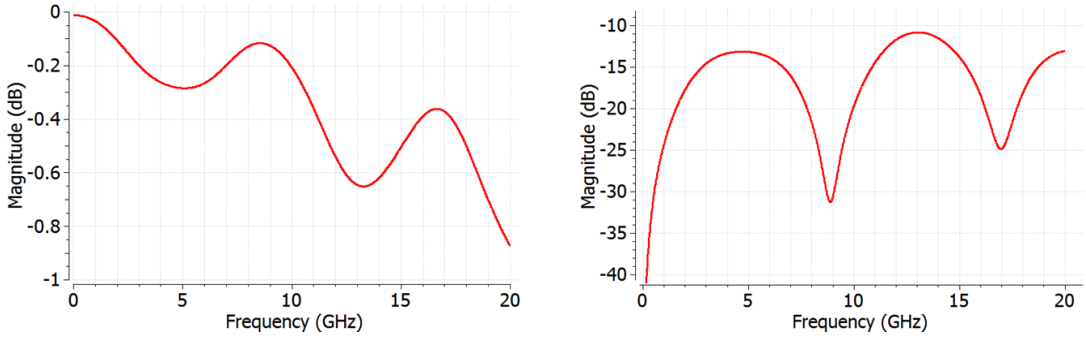

(a) (b)

Figure 2.5. Full wave modeling results for (a) $|S_{dd21}|$ of the transition, (b) $|S_{dd11}|$ of the transition.

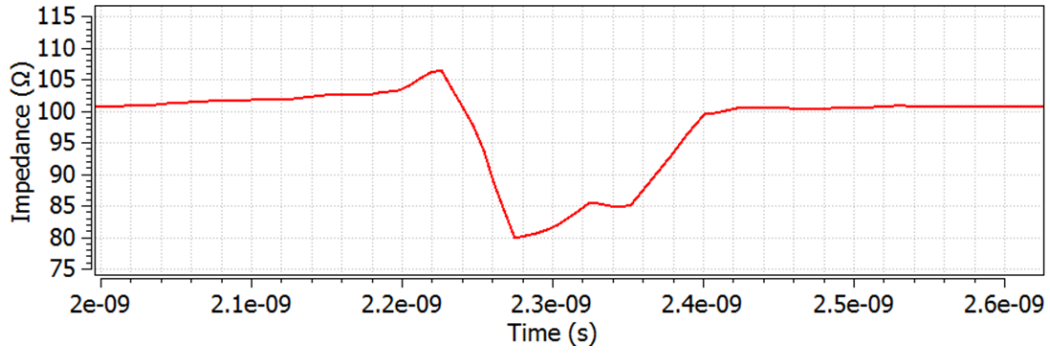

(c)

Figure 2.6. Full wave model simulation results for differential TDR.

The differential mode TDR response, as shown in Figure 2.6 is also used to guide the engineering of the transition. Even though there is an impedance mismatch between the trace and the probe, the extra impedance variation from 100 Ω to 85 Ω is well controlled at less than 5 Ω from the differential mode TDR. The response from 2.3 ns to

2.4 ns corresponds to the differential pair with characterized impedance of 85 Ω. The impedance at later times is 100 Ω because of the settings in the commercial modeling tool during the TDR calculation.

2.3. THE TEST VEHICLE DESIGN AND MEASUREMENT

The geometry determined from full wave modeling is used, and a 16 layer printed circuit board (PCB) with the unified probe launch pattern is designed and manufactured as shown in Figure 2.7. In this board, 3 routing lengths, 2 inch, 5 inch, and 10inch differential pairs are located in the top layer, and layers 10, 12 and 14. The 10 inch differential pairs are the DUT during the de-embedding calculation.

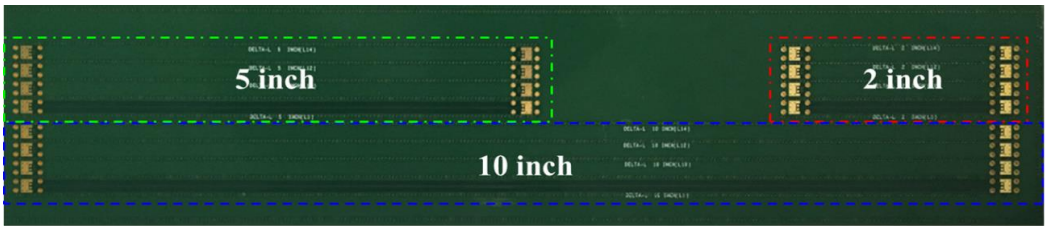

(a)

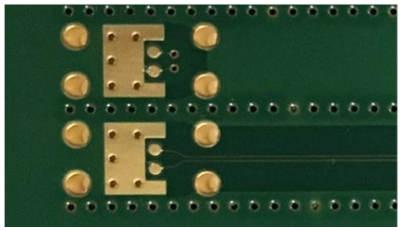

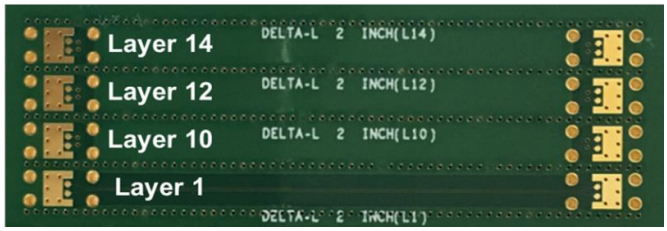

(b) (c)

Figure 2.7. (a) Top view of the test vehicle and (b) zoomed in view of the unified probe launch pattern, and (c) the routing view of the 2 inch differential pairs.

The 2 inch and 5 inch differential pairs are used as the 2x thru references to do the de-embedding and remove the fixture with the de-embedding method, leaving an 8 inch or 5 inch differential pair to do the DK and DF extraction. A 10 MHz to 20 GHz four-port measurement is done with the differential probe as shown in Figure 2.8(a). In Figure 2.8(b), the differential probe landing with the metal base is shown, whose four guide pins provide for easily landing the probe on the probing pad in an efficient and repeatable manner.

After 4-port SOLT calibration, the differential probes are connected to the precision cable and landed on the test vehicle to do the S-parameter measurements. The measured S-parameter results with SOLT calibration, on layers 10 12 and 14, for the 2 inch differential traces are shown in Figure 2.9 as an example.

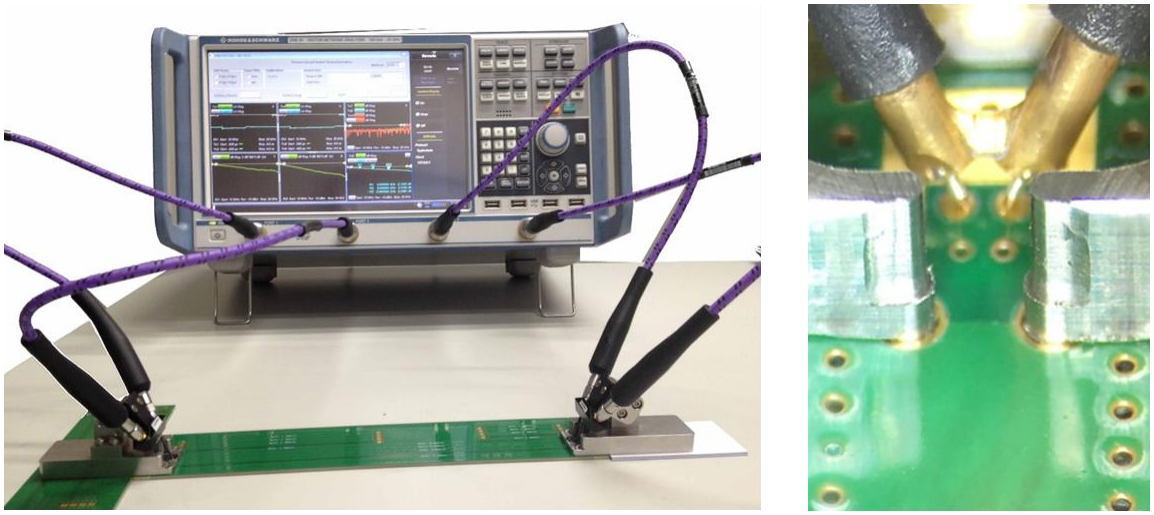

(a) (b)

Figure 2.8. (a) 4-port measurement setup and (b) probe landing photo showing the SS probe and the mechanical base with guide pins in the foreground.

From the S-parameter comparison, there are some ripples caused by the impedance mismatch between the differential pair and the probe. And the amplitude of the functional variation for the Layer 10 result is greater than the others because of the longer via stub, as can be seen from the differential TDR shown in Figure 2.10 for the 2 inch differential pair for layers 10 12 and 14.

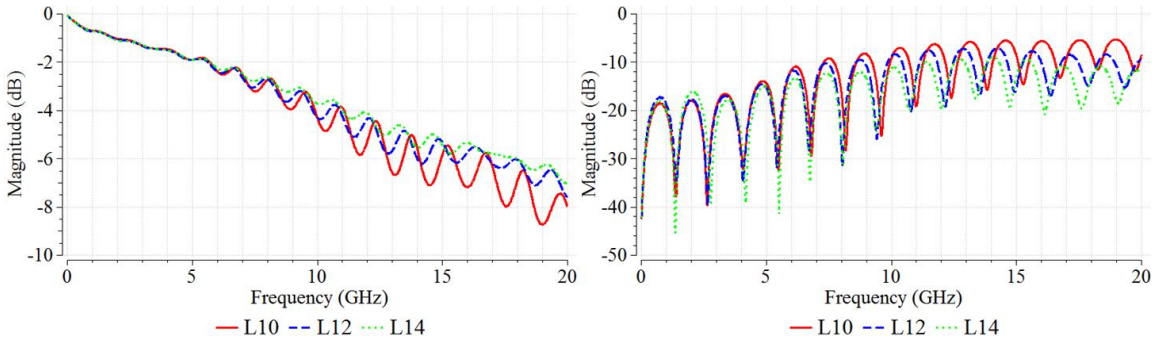

(a) (b)

Figure 2.9. (a) Layer 10 12 and 14, 2 inch differential pairs $|S_{dd21}|$, and (b) $|S_{dd11}|$.

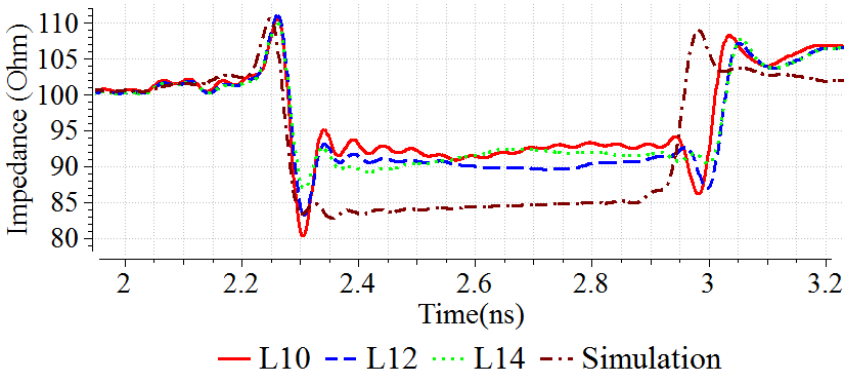

Figure 2.10. 2 inch differential trace differential mode TDR at layer 10, layer 12, and layer 14, and comparison with the layer 12 simulations.

SOLT calibration at the cable ends was used for the S-parameter measurements, and then an inverse Fourier transform to get the time-domain results. The layer 12 simulation calculations of the differential mode characteristic impedance is also added for comparison with the measurements and corroborating the simulation.

The manufactured PCB did not achieve the specified 85 Ω, as seen in the Figure 2.10 TDR results, and there is an impedance difference between the simulation and measurement results. There is a 0.1 ns time delay difference between the simulations and measurement results which is caused by the different trace lengths. In the measurement, the actual differential pair length is 2118 mil which is longer than the simulation. Nevertheless, the measurement impedance of transition part is matched well with the simulation.

2.4. DE-EMBEDDING RESULTS AND DK DF EXTRACTION

A new de-embedding method denoted Smart Fixture De-embedding (SFD) is used for de-embedding the fixture part of the device under test [5].

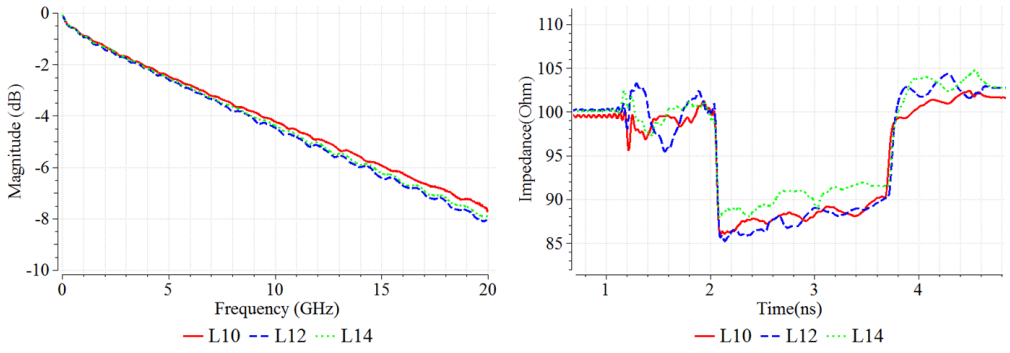

(a) (b)

Figure 2.11. (a) 5 inch differential pair $|S_{dd21}|$ after SFD, and (b) differential TDR.

For the test vehicle, the raw S-parameters of the10 inch differential pairs are the DUT and the raw S-parameters of the 2 inch, and 5 inch pairs are used as the 2x thru reference to de-embed the fixture part included the differential probe, transition parts and a small length of the differential pairs. Thus, the S-parameters of 8 inch and 5 inch differential pairs without the fixture artifacts can be extracted.

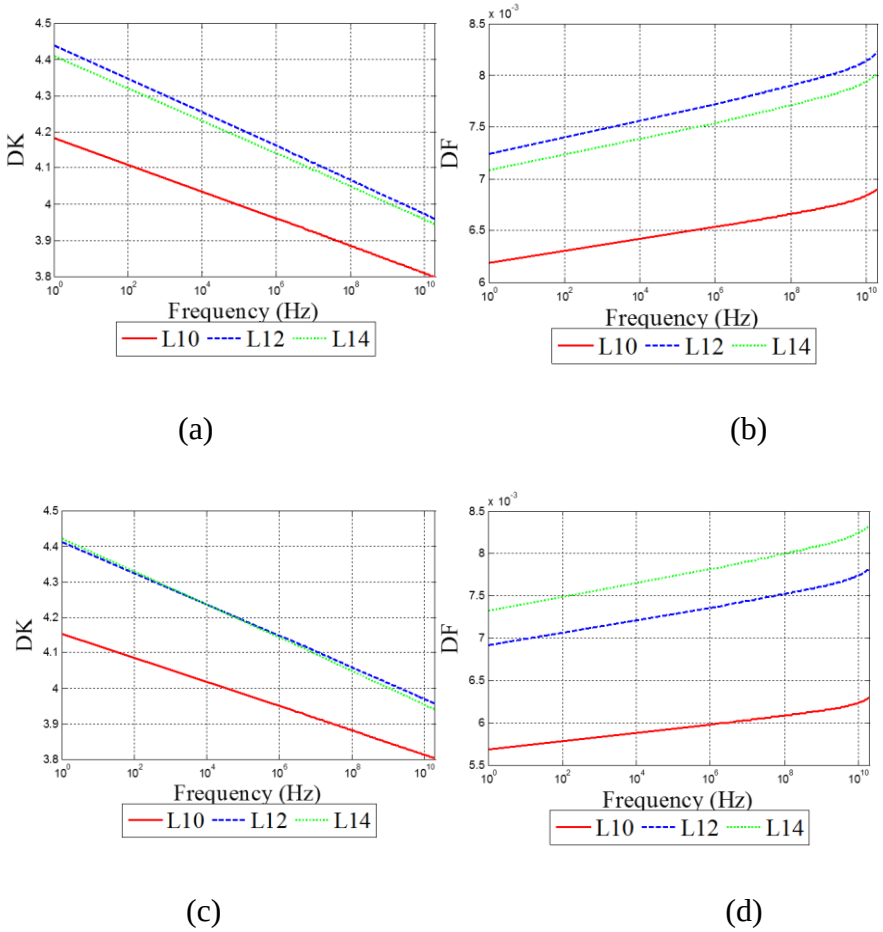

Figure 2.12. (a) and (b) the 5 inch differential pair DK and DF, (c) and (d) the 8 inch differential pair DK and DF.

In Figure 2.11, the 10 inch and 5 inch differential pairs are used to get the 5 inch DUT after de-embedding. The $|S_{dd21}|$ of the 5 inch de-embedded differential pairs are shown in Figure 2.11. (a). Small ripples of the $|S_{dd21}|$ are from the 90 Ω differential impedance. The insertion loss of the differential pair at Layer 10 is less than the other layers due to the manufacturing of the PCB.

The S-parameters after SFD are used to do the DK and DF extraction [6-9]. An algorithm for DK and DF extraction is provided based on the $|S_{dd21}|$ and $|S_{cc21}|$ of the differential pair [10]. The results of the DK and DF extraction from the 8 inch and 5 inch DUT are shown in Figure 2.12.

The DK and DF results show that the Layer 10 results have less loss than the other layers. From the comparison of the DK with different lengths, the extracted DK for the 8 inch and 5 inch DUT are very consistent. The DF results also show the same consistency in the results between the 5 inch and 8 inch DUT.

3. UNIFIED PROBE LAUNCH PATTERN – 0.5 MM PITCH

A high-frequency microprobe for measurements up to 40 GHz was designed using a 0.5 mm probe pitch. Thus, to accommodate the higher frequency probe transition, several portions of the probe launch geometry are changed, the Figure 3.1.

For the 0.5 mm pitch probe launch pattern, not only the signal pad pitch is reduced to 0.5 mm, but the shape of the signal pad is changed to a rectangle for better transition parasitic control as well. The air gap from the U-shape ground plane to the signal pad is less than the 8mil to make sure that the ground pin of the probe lands well.

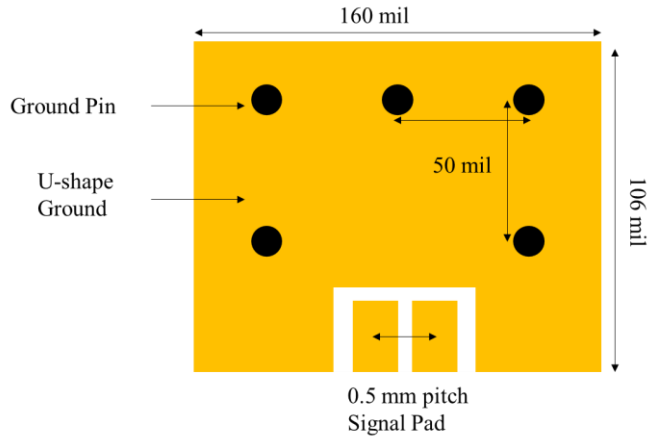

Figure 3.1. 0.5 mm pitch unified probe launch pattern dimension.

3.1. FULL WAVE MODEL DESIGN AND FREQUENCY EXTENSION

Due to the probe pitch and launch pattern changing, the full wave model is modified in several parts. Firstly, the previous 1 mm pitch differential probe is changed to a new 0.5 mm pitch probe, and the model is developed for the full wave simulation.

For the new probe as shown in the Figure 3.2, the coaxial parts are kept as before, but the landing portion is different. Two ground pins are added for measuring the common mode S-parameters and the two blade ground blocks attached on the ground pin are used to reduce the inductance between the probe tips and launch pattern. Several additional modifications to the transition are made as well to improve the performance.

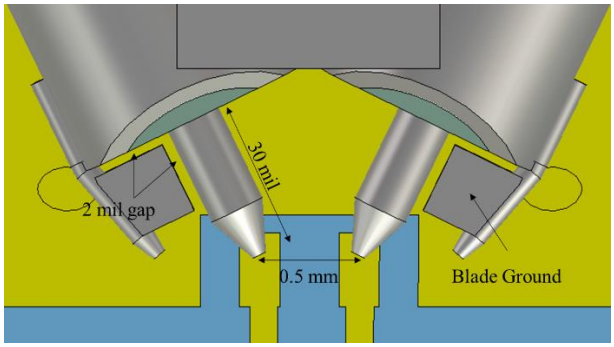

Figure 3.2. Schematic diagram for the probe landing dimensions.

In the 1 mm pitch probe launch, the via stubs were not back-drilled, which limited the frequency range. However, for performance up to 40 GHz, the via stubs must be back-drilled to achieve adequate high frequency performance [11]. In the new transition section, the additional via stubs were removed to simulate back-drilling, and the results with and without the back-drill are shown in Figure 3.3. (a). From the $|S_{dd21}|$ comparison, the back-drilling dramatically improves the transition performance beyond 25 GHz. Additionally, two ground vias are added beside the pair of signal vias, to achieve better high frequency performance [12]. Because of the two ground vias, a near current return path is used for tuning the parasitics of the via. In Figure 3.3. (b), with the ground vias, the $|S_{dd21}|$ has a smoother functional variation from 25 GHz to 35 GHz.

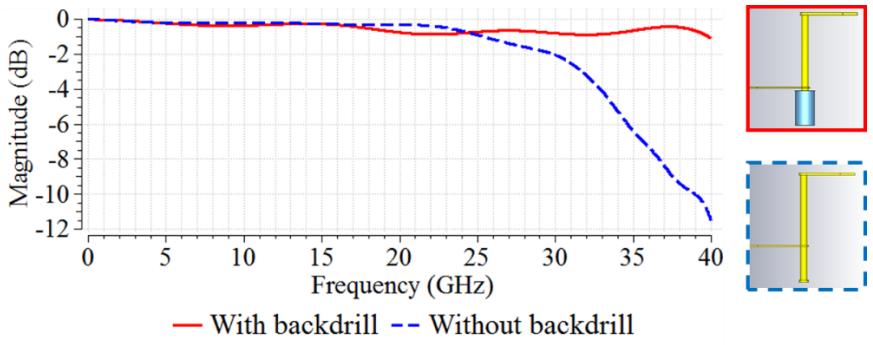

(a)

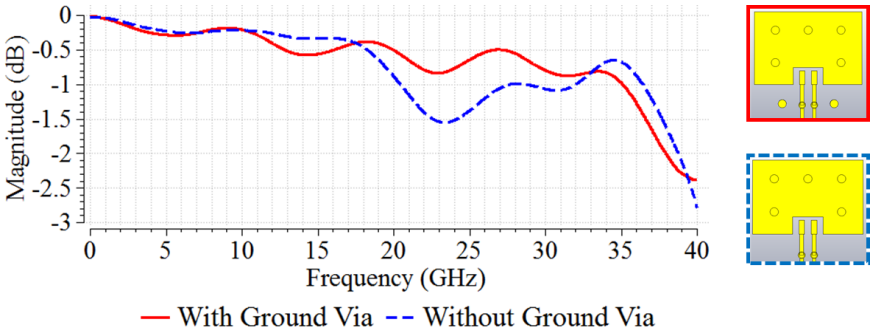

(b)

Figure 3.3. (a) Transition with and without back-drill $|S_{dd21}|$ and (b) with and without ground via transition part $|S_{dd21}|$.

Including the two primary modifications noted above, and several geometry optimizations, the full wave model and dimensions are shown in Figure 3.4. In this model, the same 16 layer PCB stackup and design as in Section 2 is used. The total width and length of the simulated transition are 250 mil and 500 mil. A detailed top view of the landing geometry is shown in Figure 3.4. (a). The four guide pins holes remain to facilitate precise and repeatable probe landing. A side view of the transition is shown in Figure 3.4. (b). The differential impedance of the differential stripline pair is controlled for 85 Ω with strong coupling, and the length of the differential pair is 230mil.

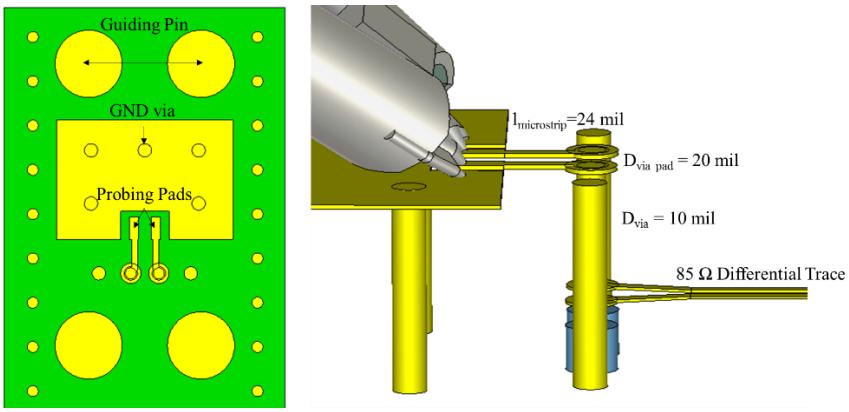

(a) (b)

Figure 3.4. (a) Top view of the unified probe launch pattern and (b) side view of the transition model and dimensions.

The differential pair modeled is at Layer 10. The S-parameters and calculated TDR from the S-parameters are shown in Figure 3.5. From the simulation results, the insertion loss of the 0.5 mm unified probe launch pattern transition model is less than 1.2 dB and the return loss is approximately 13 dB at 40GHz, which is very close to the simulation results of 1 mm pitch probe launch pattern transition model at 20 GHz. In other words, based on the previous experience, the simulation transition performance of the 0.5 mm pitch probe landing fixture should work up to 40 GHz.

In the TDR results, the differential impedance variation at the probe tips, from 2.2 ns to 2.25 ns, is less than 105 Ω on an impedance scale, and then with the via impedance change the characteristic impedance smoothly transitions to the 85 Ω, which is the differential stripline pair impedance.

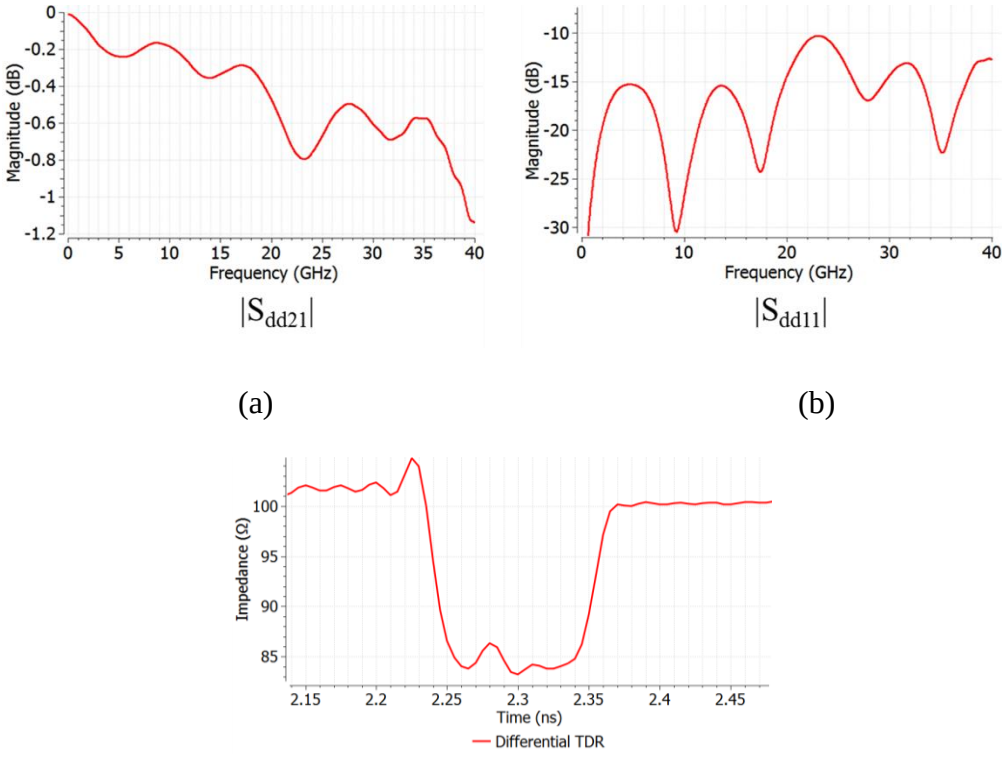

Figure 3.5. (a) Full wave transition model $|S_{dd21}|$and (b) $|S_{dd11}|$, and (c) the calculation differential TDR.

3.2. DIFFERENT PROBE LANDING STUDY

Different probe grounding strategies were simulated based on the new 0.5 mm GSSG probe design. Four different grounding strategies were investigated. The differences among the four cases are the length of the probe tips, different ground probe patterns, and the different angles, 60º and 45º of probe landing.

The simulated results for the four probes are shown in Figure 3.6. The first probe with the two ground pins and 30 mil length signal tip lands on the probe launch pattern with a 60º angle. Based on the first probe, the probe tip length is reduced to 20 mil and

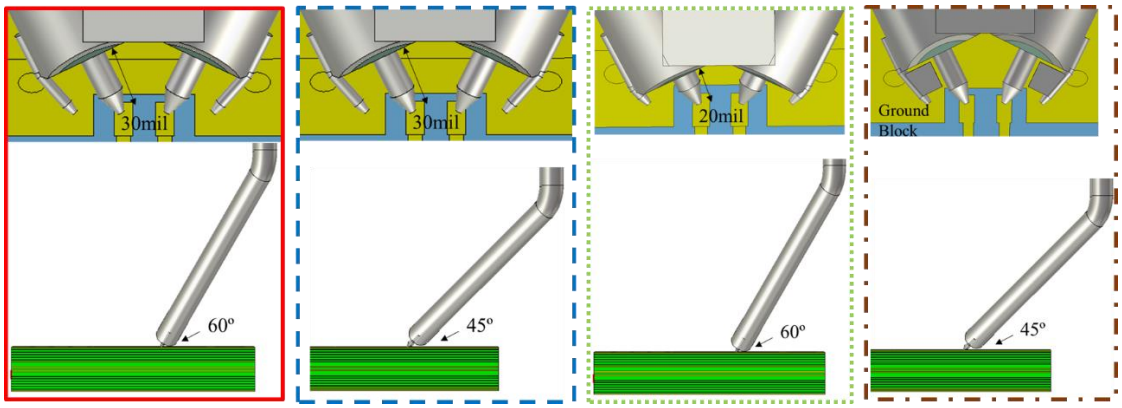

(a) (b) (c) (d)

Figure 3.6. (a) 60º landing angle and 30 mil tip probe, (b) 45º landing angle and 30 mil tip probe, (c) 60º landing angle 20 mil tip length probe and (d) 45º landing angle and blade ground probe.

the landing angle is kept. For the third probe, the tip length is kept as 30mil but the probe landing angle is changed to 45º. The fourth probe is the one which is used in the final transition model, the 45º probe with blade ground pin.

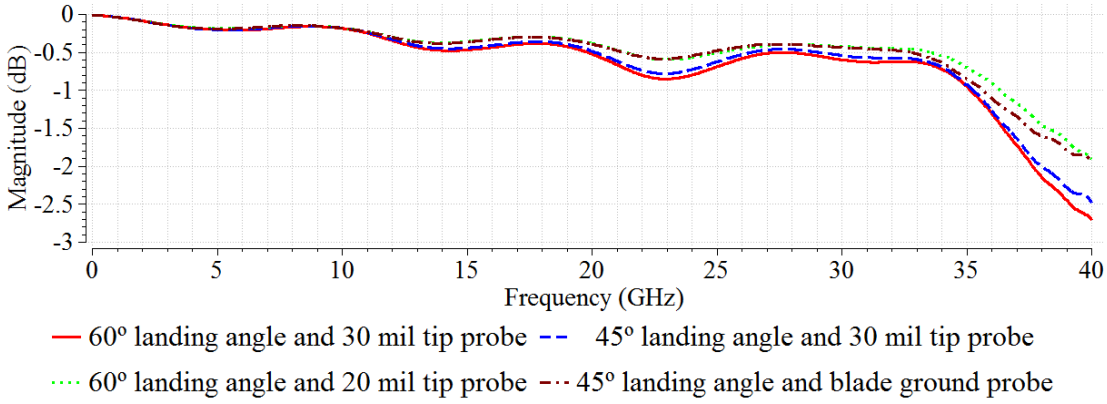

Figure 3.7. $|S_{dd21}|$ for the four different 0.5 mm pitch probes.

In the TDR curve in the Figure 3.8, the differential impedance from the 2.23ns to 2.25ns correspond to the probe tips and landing portion. For the 20 mil tip case, the short tip decreases the inductance between the probe and launch pattern.

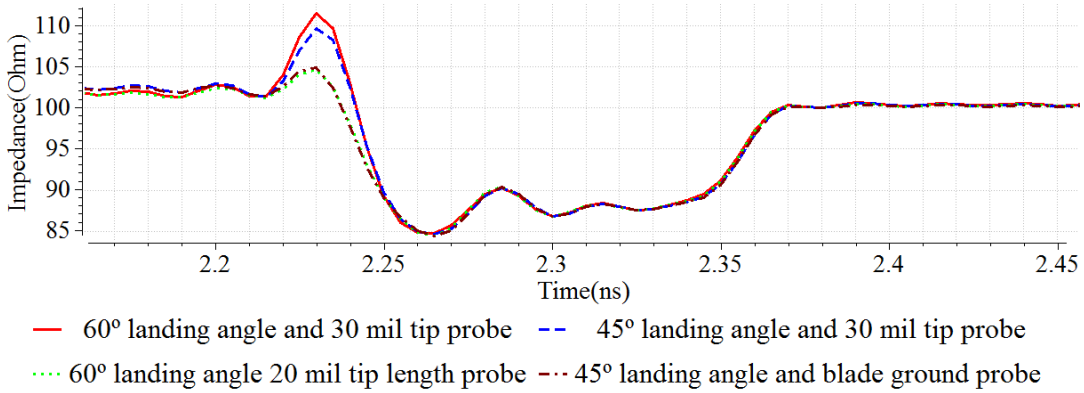

Figure 3.8. Differential TDR for the four different 0.5 mm pitch probes.

Even the worst case, the probe with 30 mil tip length and 60º landing angle, the performance of the transition part is still such that the insertion loss is less than 2 dB up to 38 GHz as shown in the Figure 3.7.

3.3. TEST VEHICLE DESIGN

In the last test vehicle, only the probe portion is considered and designed. For the 0.5 mm unified probe launch pattern, for increasing measurement accuracy, a 2.92 mm connector differential S-parameters measurement is also needed as a golden standard to verify the SFD and DK, DF extraction results from the probe measurement as shown in the Figure 3.9.

In this test vehicle design, the same 16 layer stack-up is used as described in Section 2. Three trace routing lengths of 2 inches 5 inches and 10 inches are used in the test vehicle for probe and connector measurement. Layers 1, 10, 12 and 14 are used for routing traces in the same way as the previous test board.

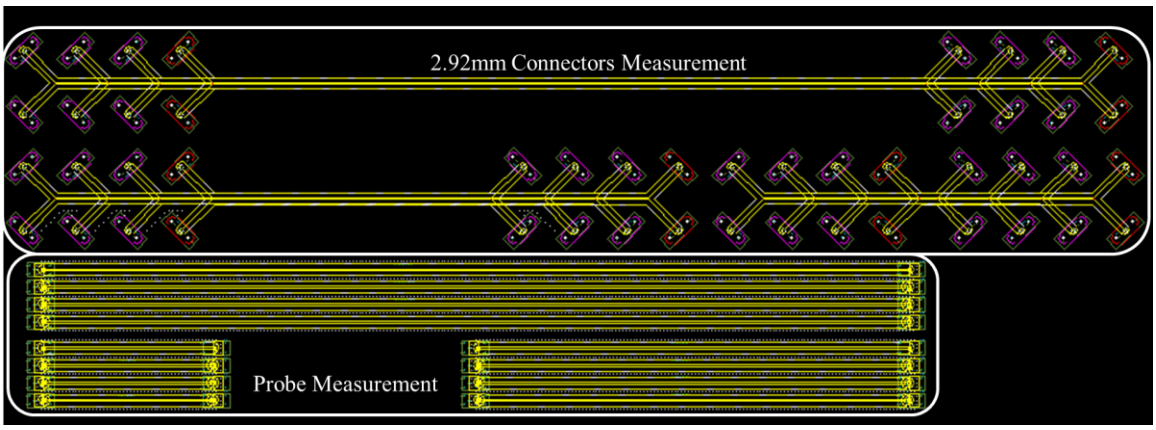

Figure 3.9. 0.5 mm probe launch pattern test vehicle layout.

For the DK and DF extraction algorithm, several algorithms are used to extract the printed circuit board material properties. The most common way uses the $|S_{dd21}|$ of the differential pair after de-embedding to do the extraction. However, these algorithms inherently include the surface roughness losses in the extraction results, and effects the assessment of DF.

In this design, a new algorithm is used that includes measurement of $|S_{dd21}|$ and $|S_{cc21}|$ of the differential pair after de-embedding. Using both, the surface roughness loss can be separated from the dielectric losses and excluded DF results. To achieve this objective, the 85 Ω differential pair is strongly coupled so that the differences between the $|S_{dd21}|$ and $|S_{cc21}|$ can be used to do the extraction.

The board stack-up table will be attached in the appendix. The working layers are same as the 1mm pitch probe testing board, layer 10, layer 12 and layer 14. The transmission line at layer 10 has asymmetry stack-up design. The above material thickness is 10mil and the below material thickness is 3mil. The transmission lines at layer 12 and layer 14 have symmetry design but different thickness. The material thickness of layer 12 is 5mil and the material thickness of layer 14 is 4mil. In this way, the differential characterize impedance of different layer are not identical.

3.4. TESTING VEHICLE BOARD MEASUREMENT RESULTS

Based on the design of the testing vehicle, several testing PCB boards are manufactured as shown in the Figure 3.10. . Two sets of testing methods are measured, the 0.5 mm probe launch pattern and the 2.4 mm top mount connectors to verify the accuracy of probing measurement.

Figure 3.10. 0.5 mm pitch probe lunch pattern testing board.

From the measurement $|S_{dd21}|$ as shown in the figures, the curve are smooth and linear up to 30 GHz, then an unexpected dip occurred due to the angel of glass wave which will be discussed later.

3.4.1. 0.5 mm Probe Measurement Results. From the Figures 3.11 to 3.13, the measurement results reveal the similar tendency in different trace lengths. At the layer 10, the differential characterize impedance is 90 Ohm and the differential characterize impedance is dropped down to 80 Ohm at the layer 12 and layer 14 which is due to the different stack up design as shown in the previous testing fixture design.

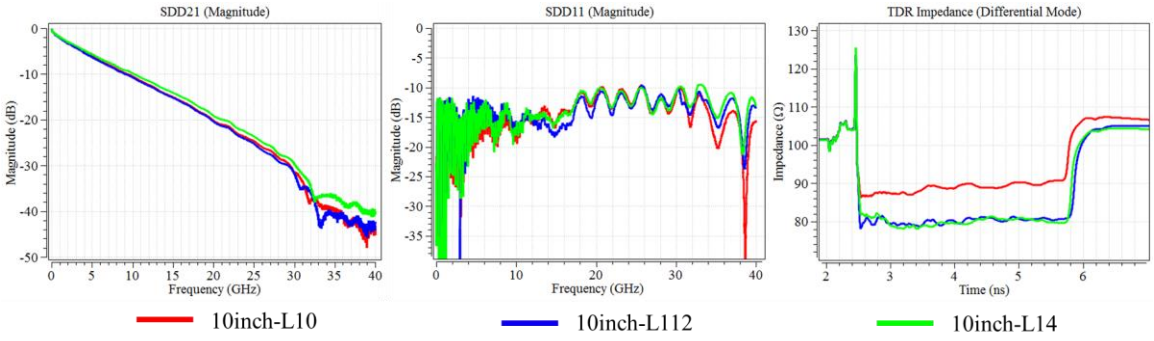

Figure 3.11. Differential probe measurement results of 10 inch traces at different layer.

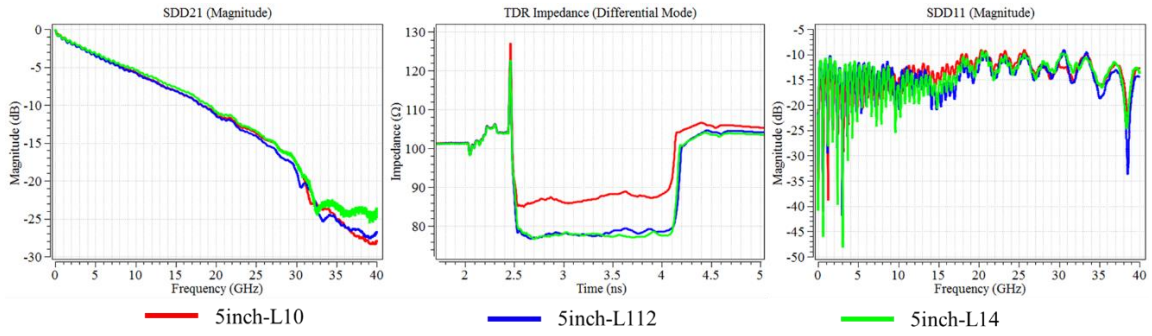

Figure 3.12. Differential probe measurement results of 5 inch traces at different layer.

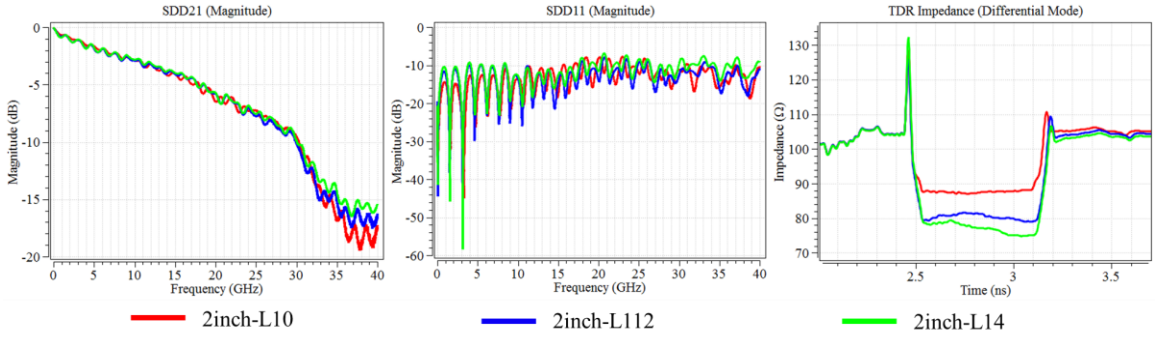

Figure 3.13. Differential probe measurement results of 2 inch traces at different layer.

From above Figures, 3.11 - 3.13, the measurement results reveal the similar tendency in different trace lengths. At the layer 10, the differential characterize impedance is 90 Ohm and the differential characterize impedance is dropped down to 80 Ohm at the layer 12 and layer 14 which is due to the different stack up design as shown in the previous testing fixture design.

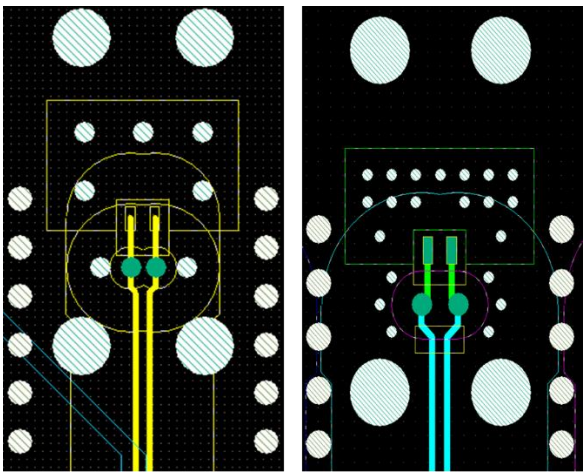

Figure 3.14. Probe landing pattern and transition modification.

Except the variance of differential characterize impedance, the consistency is shown as well. All the results regardless of the layers and length show that a unexpected dip of insertion loss after 30GHz. The dip is considered as a glass fiber effect due to the manufacturing which would be further discussed later.

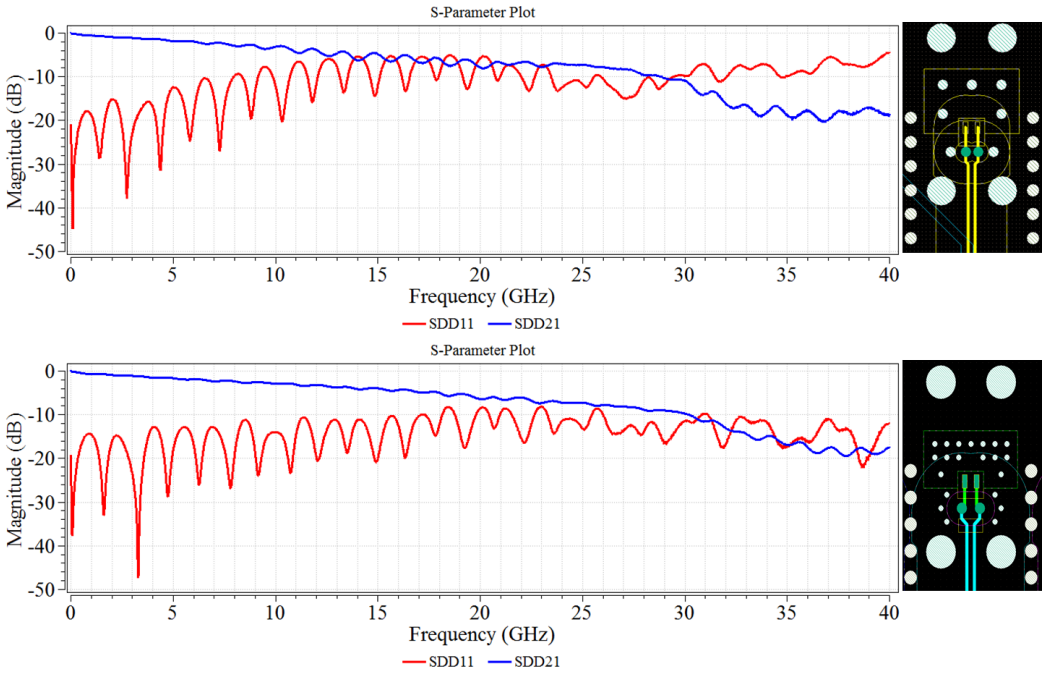

Figure 3.15. The $|S_{dd21}|$ and $|S_{dd11}|$ comparison between the two versions of probing landing testing PCB boards.

There are two versions of PCB board are manufactured based on the original testing board design as shown in the Figure 3.14. The landing pad and transition portion are improved in the second version and the above results is from the second version of board manufacturing. In the version 2, more ground vias are added to reduce the length of return path. Then the differential vias of transition is re-designed for getting better impedance control as shown in the Figure 3.15. The spacing between the transmission

line and same layer ground is enlarged as well for getting better DK and DF extraction results.

According to the IEEE p370 de-embedding standard, the de-embedding frequency range is decided by the loss cross point between the insertion loss and the return loss. As shown in the S-parameters plot. In Figure 3.15., the above figure is the old version, the cross point is at 15GHz, and the below figure shows the cross point is pushed to 30GHz with the new design.

3.4.2. Top Mount Connector Measurement Results. Besides the probing measurement, the same length traces with the 2.4 mm connector are add. Those portion is used to verify the results of probing measurement. The de-embedding results between the probing and connector should be identical due to the similarity of trace design.

From the Figure 3.16-3.18, the insertion loss and return loss works smoothly up to 30GHz. Then an unexpected dip of insertion loss show up which is corresponded to the probing measurement results. According to the previous paper, the dip is highly possible from the issue of glass wave bundle.

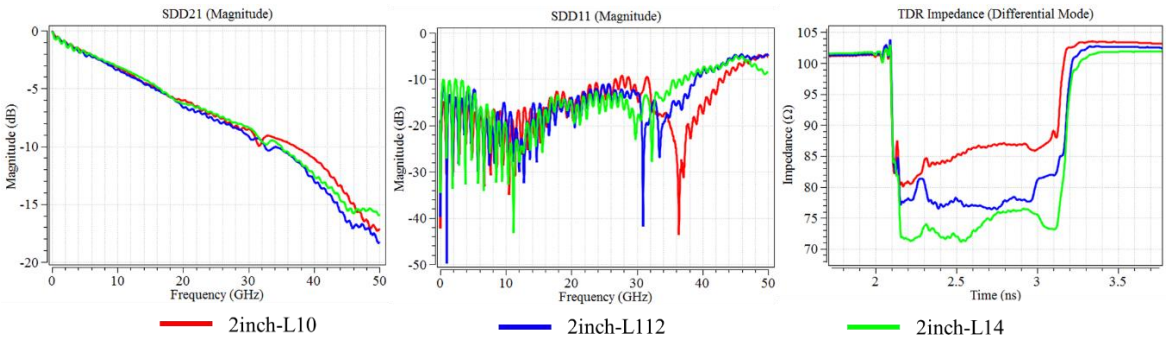

Figure 3.16. 2.4 mm connector measurement results of 2 inch traces at different layer.

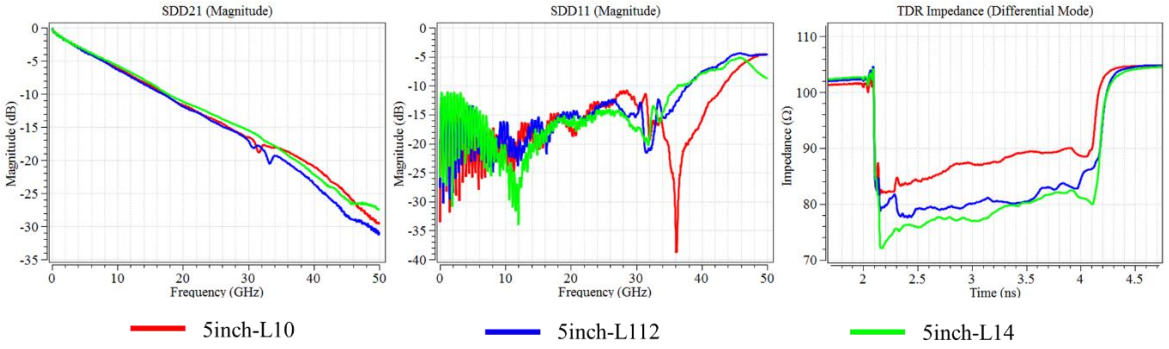

Figure 3.17. 2.4 mm connector measurement results of 5 inch traces at different layer.

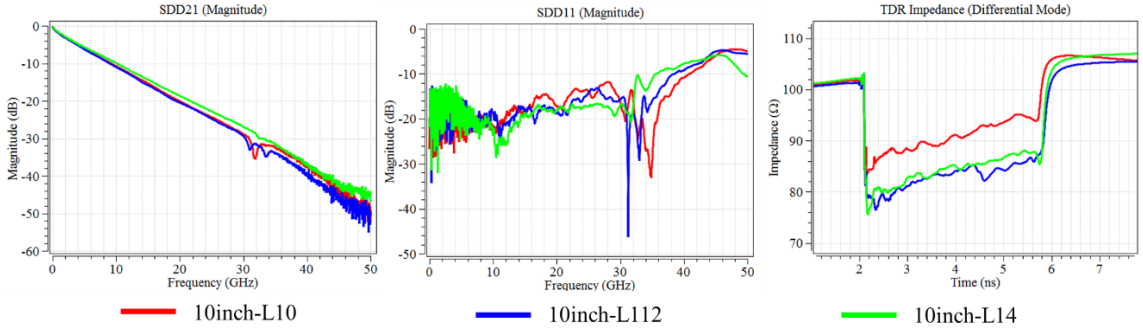

Figure 3.18. 2.4 mm connector measurement results of 10 inch traces at different layer.

From the Figure 3.19, it prove the hypothesis that the dips aren't from the design but from the manufacturing is proved. The dip occurs at the different length of trace at the same layer no matter what measurement method is used. Therefore, in the future version, the angle between the trace and the glass wave bundle should be carefully considered. Several degrees rotation of design are necessary for avoiding the dip issue at high frequency.

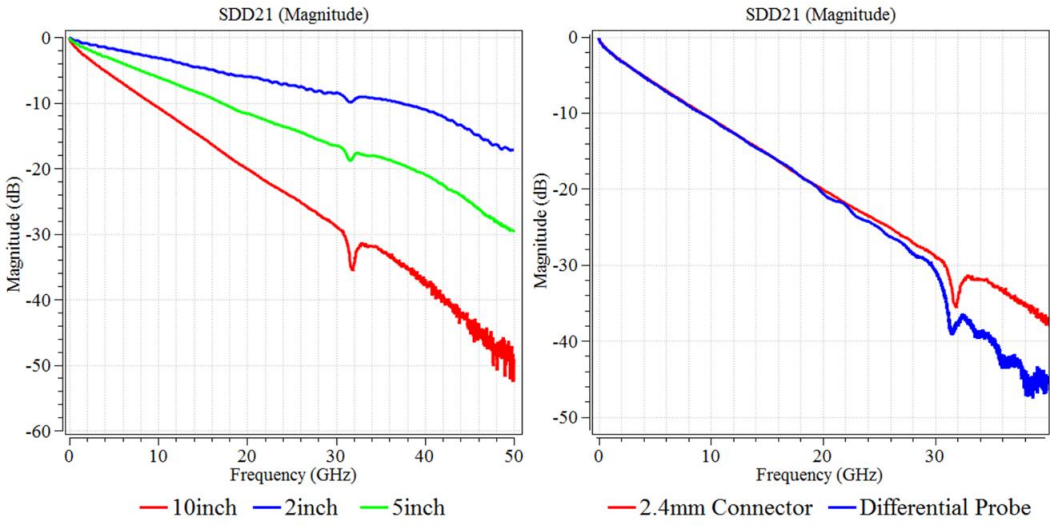

(a) (b)

Figure 3.19. (a) Measurement results of different length at same layer 10 with 2.4 mm connector, (b) measurement results of different method at same layer 10 and same PCB board.

3.4.3. De-embedding Results with Smart Fixture De-embedding Tool. In this portion, the de-embedding method is from the previous studying. In this method, two S-parameters are needed for de-embedding, the 2X thru and the DUT with fixture. In this case, the 10inch trace plus the connector or differential probe is the DUT with Fixture. And the 5inch or 2inch traces with fixtures are the 2X thru.

The fixture includes differential probe or 2.4mm top mounting connector and the transition portion like the landing pad and signal vias. Figure 3.20 is the probing measurement results. It shows that the de-embedding results are good at three layers up to30 GHz, then an unfriendly dip occur after 30 GHz. Regardless of the dip, three layers are consistent and smooth.

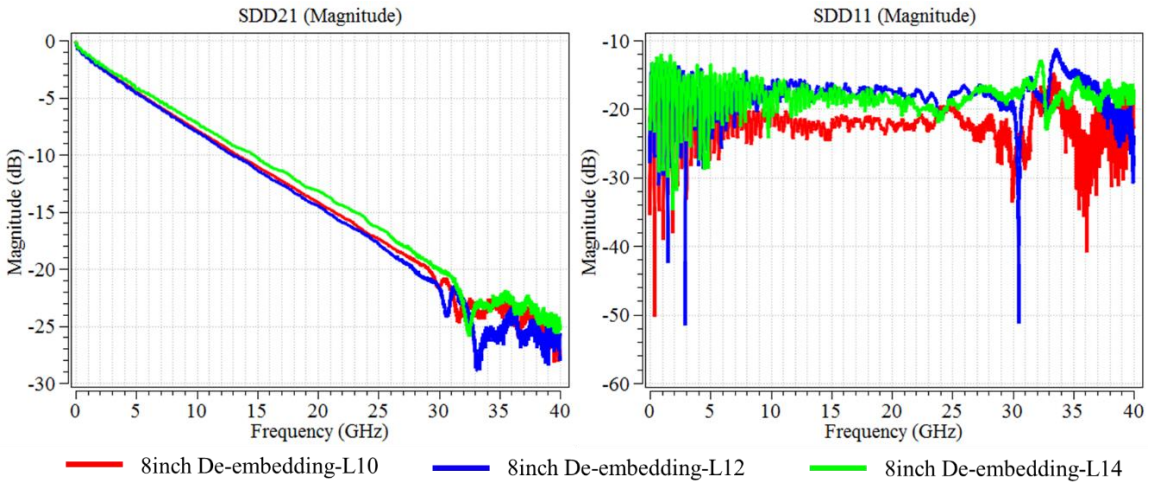

Figure 3.20. Probe de-embedding S-parameters at different layers.

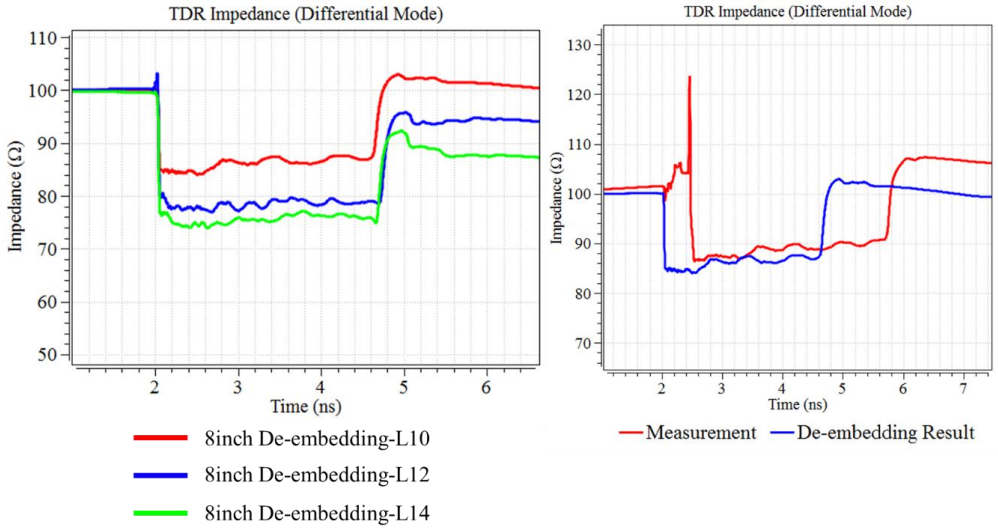

(a) (b)

Figure 3.21. (a) De-embedding TDR impedances at different layers, (b) TDR impedance comparison within measurement results, the 10 inch trace at layer 10 and de-embedding results of 8 inch transmission line.

The de-embedding results of 2.4mm connector, Figure 3.21 and Figure 3.22 show the same behavior as the probing measurement due to glass wave bundle. The dip shows

at the same frequency point as the probing measurement, which means the dip isn't from the probe and connector measurement. It should be from the manufacturing.

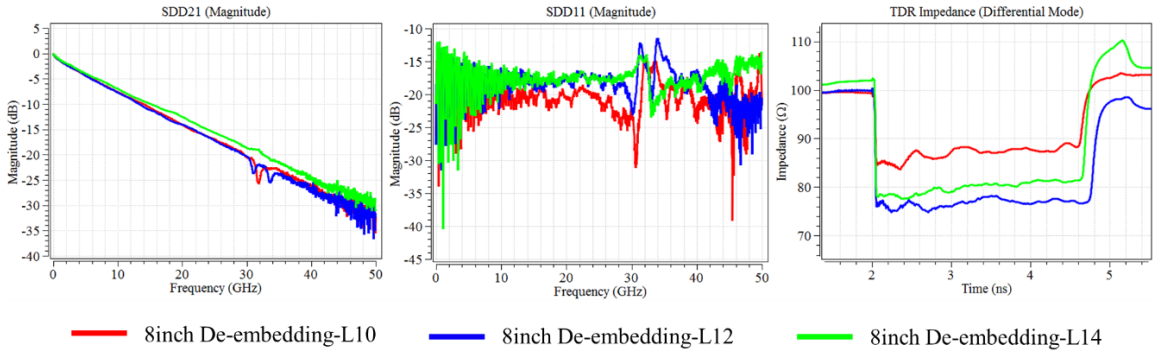

Figure 3.22. 2.4mm connector de-embedding S-parameters at different layers.

The Figure 3.23 shows that the same features between the two measurement methods after de-embedding. The differential impedance is around 85Ohm and the insertion loss and return loss are correlated to each other. The de-embedding results will be used as the input data for PCB measurement characterization.

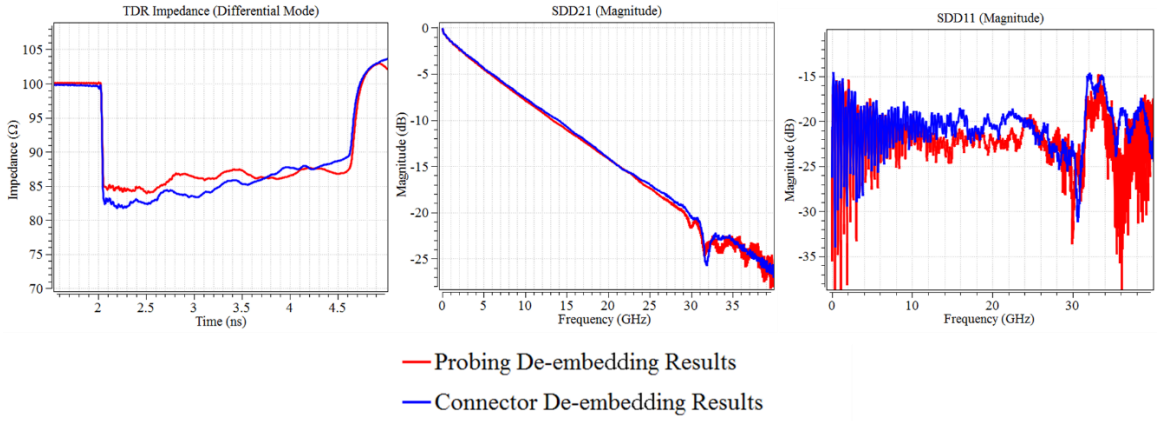

Figure 3.23. The comparison between the probing and connector de-embedding results.

3.5. DK AND DF EXTRACTION RESULTS

As mentioned DK and DF extraction method before, a PCB cross-section extraction is done in Figure 3.24 for getting the accuracy trace and stack-up dimension.

Table 3.1 is one of the board dimensions from the PCB board cross-section. The material extraction tool use the dimension and the de-embedding S-parameter to extract the DK and DF results.

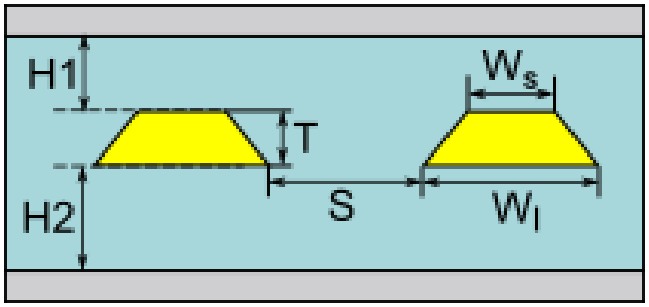

Figure 3.24. The essential factors of PCB cross-section.

Table 3.1. Testing board stack up at layer 10.

Input stack-up	Dimensions(mil)	Input stack-up	Dimensions(mil)
Trace-width(W_l)	5.39	Trace spacing(S)	6.99
Trace-width(W_s)	4.41	Above height(H1)	10.75
Etch factor(E)	0.49	Below height(H2)	2.81
Trace Thickness(T)	1.26		

3.6. EXTRACTION RESULTS ANALYSIS

The Table 3.2 shows extracted DK Df and surface roughness results. From the table, the DK and Df with different measurement method have the closely results. The DK difference is less than 2% and the difference of Df is less than 5%. The roughness level is defined in the reference. The lower number means the smooth surface. Usually, the -2 roughness level and -1 roughness level means the same surface roughness like VLP (Very Low Profile). In this way, the results prove that the probing measurement at high frequency still can be used for doing PCB material characterization.

In the future, a new version will be released for fixing the glass wave bundle issue. At that time, the probing method should work up to 40GHz or higher depends on the probe quality.

Table 3.2. The DK Df extraction results and surface roughness level.

	DK at 1GHz	Df at 1GHz	Surface roughness level
L10 D-probe	3.77	0.0082	-1.02
L12 D-probe	3.99	0.0081	-2.31
L14 D-probe	3.85	0.0078	-2.29
L10 Connector	3.72	0.0086	-0.91
L12 Connector	4.1	0.0081	-1.78
L14 Connector	3.82	0.0077	-1.08

3.7. RESULTS SUMMARY AND ANALYSIS

In this section, the 0.5mm probe unified probe launch pattern design and testing fixture design is addressed. The design of 0.5mm pitch unified probe launch pattern is inherited from the 1mm pitch unified probe launch pattern with higher working frequency range and better utility. The testing board design improved the 1mm pitch testing board and the push the frequency range to 40GHz or higher. Nevertheless, the unexpected boarding manufacturing issue stop the achievement. Even the dip appears frequently and hard to remove, the de-embedding results still smoothly work up to 30GHz. And the DK and Df and surface roughness extraction has good identity with different measurement method.

4. PROBING S-PARAMETER AND MODELS EXTRACTION

4.1. METHOD INTRODUCTION

In this section, a new method for extracting S-parameter block of probe and landing pattern is proposed and a testing coupon is designed for verify the method. Then a full wave model and a circuit model[15-17] based on the measurement and de-embedding results[11-12] are extracted as well.

4.2. DE-EMBEDDING METHOD APPLICATION

In this part, a probe s-parameter de-embedding method is presented. According to the previous work[], the de-embedding method named SFD(smart fixture de-embedding) not only de-embed the fixture from the transmission line, but can de-embedding the transmission line from fixture. In this case, the DUT is the probe instead of the transmission like the part 2-3 of the thesis.

In this de-embedding method, the 2X thru will be divided by two from the center of the 2inch microstrip, then the 1x DUT, the probe plus the landing pattern and the 1 inch microstrip will be de-embedded with the half 2x thru S-parameter block. Finally, only the probe and probe launch pattern and a very short traces would left after complete processing. Ideally, the output of the de-embedding is the S-parameter block of the probe. The users or probe vendor could use it to qualify their probe behavior. In the future, the S-parameter block could be used as a black box when develop more probing applications. The performance of the S-parameter block should be stable and trustable.

4.3. TESTING BOARD DESIGN

There are two sets of fixture designs on the board. Each set includes two part, one is the 2 inch differential microstrip pair as known as the 2X thru, another part is the 1 inch differential microstrip pair with the probe launch pattern. Two different pitch sizes are on the board, 1mm pitch and 0.5mm pitch for two kinds of differential probe.

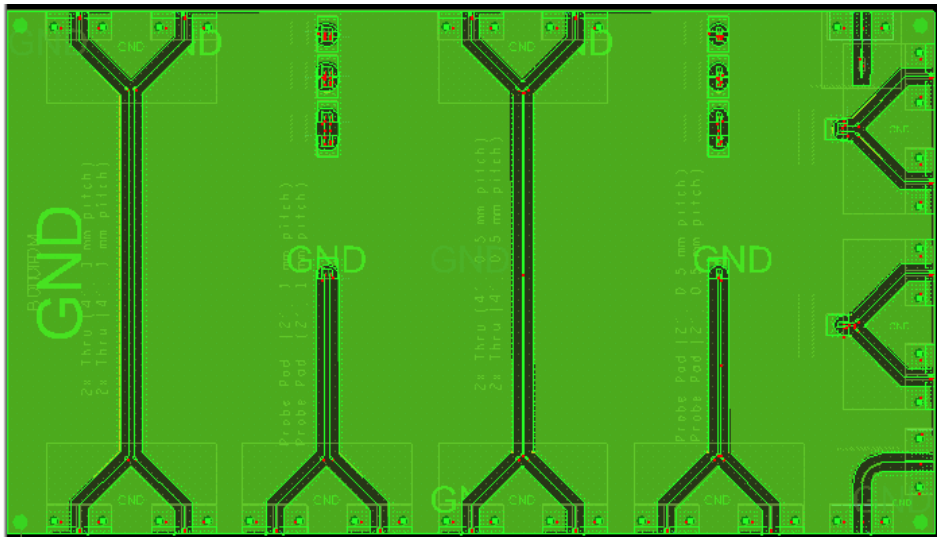

Figure 4.1. The previous design layout.

According to previous design, Figure 4.1, the length of trace (2x thru) is 4 inch which is proper for 1mm pitch probe landing. However, due to the high loss material of PCB board, the working frequency of the testing fixture is only up to 18GHz. The frequency range of 0.5mm probe is from 0Hz to 40GHz. In the new design, the maximum length of the trace is reduced to 2inch from the simulation and analysis as shown below as shown in the Figure 4.2. The board layout has the same strategy as the 4 inch case except the length of trace.

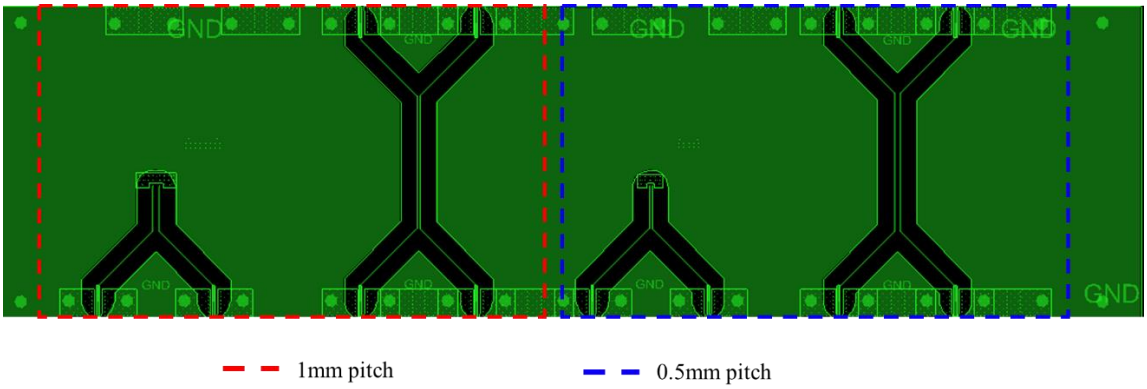

Figure 4.2. The new probe testing board layout.

4.3.1. Testing Fixture Design and Analysis. Because the measurements serve the de-embedding of probe, the quality of the 2x thru would directly effects the accuracy of the probe S-parameter extraction. In terms of the standard, IEEE P370 de-embedding standard. The low loss of testing fixture including the insertion loss and return loss would has higher de-embedding frequency range as shown in the Figure 4.3.

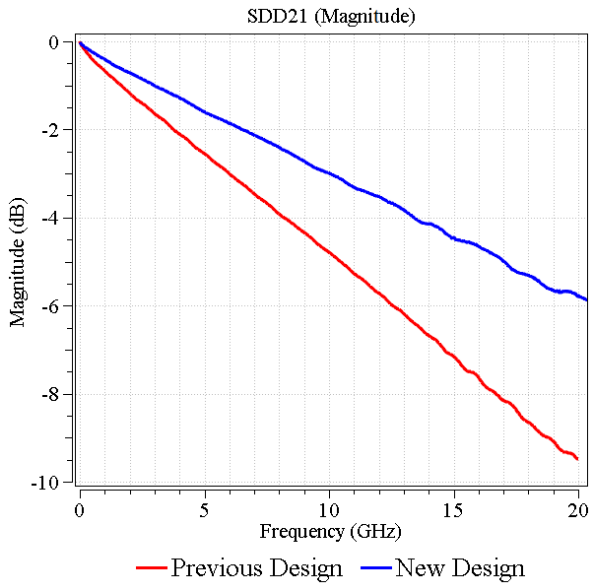

Figure 4.3. Insertion loss comparison between the previous design and new design.

From the measurement results, Figure 4.4, the cross point of $|S_{dd21}|$ and $|S_{dd11}|$ is push to 40GHz. The insertion loss is much better than the previous results.

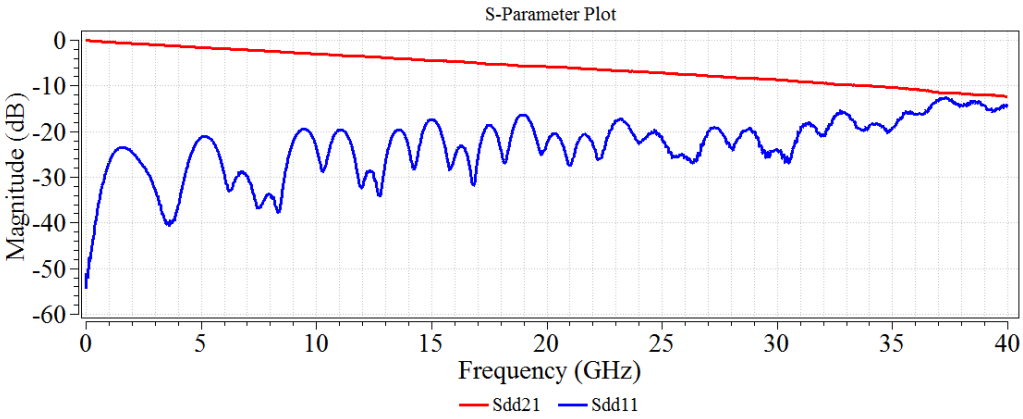

Figure 4.4. The $|S_{dd21}|$ and $|S_{dd11}|$ comparison of the new design.

4.3.2. Board Landing Pad Design. The design of probe landing pattern in this Case is shown in the Figure 4.5. In this case, the material of board is FR-4 which has higher loss but reduces the cost dramatically comparing with the testing board of unified probe launch pattern. In this way, the board could be manufactured easily and reusable.

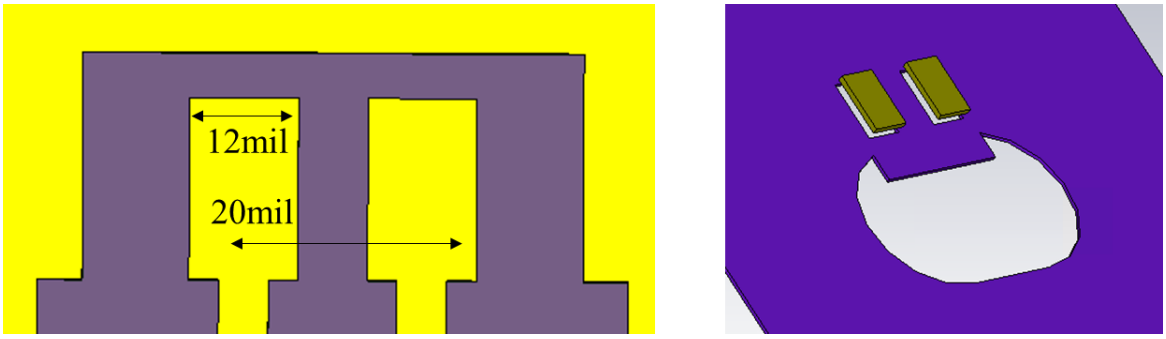

(a) (b)

Figure 4.5. (a) The pad size is enlarged to 12 mil width, (b) the slots below pad.

For achieving the acceptable behavior as the previous low loss design of the probe landing pattern, two ground slots are applied for compensating the probe effect and the mismatch between the microstrip and probe landing pad. Especially the 0.5 mm pitch probe, if the impedance from the landing pad to testing fixture has to be unified without further design, the size of landing pad would be very small which makes the landing hardly and the pad more venerable.

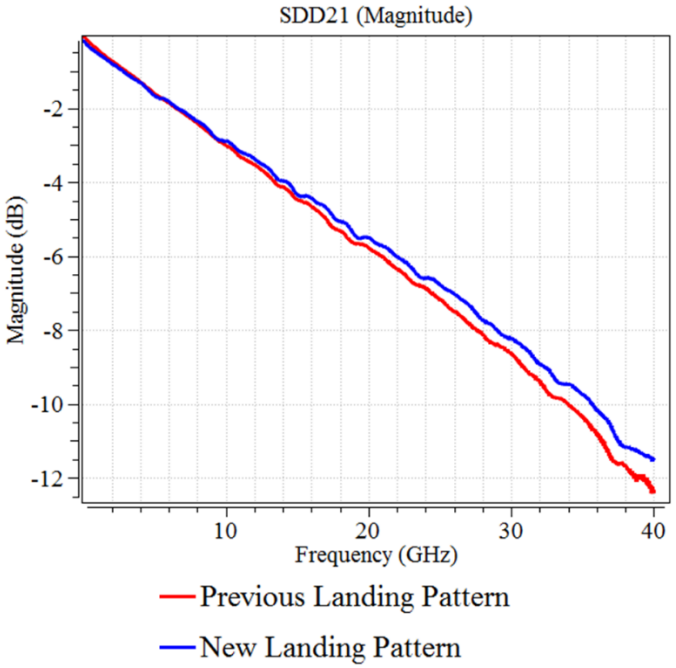

Figure 4.6. $|S_{dd21}|$ Comparison between the two designs.

Therefore, the ground slots not only improve the performance as the results shows, but make the probe landing easier. Another modification is the 4 guiding pin holes which are removed for reducing the effect from the mechanical holes to guarantee the quality of measurement as shown in the Figure 4.6.

4.4. MEASUREMENT AND DE-EMBEDDING RESULTS

The photo of differential probe, Figure 4.7, is the probe we used in the coming measurement and model extraction. The method could be used for any probe which fit with the unified probe launch pattern. As the Figure 4.8 showing, the performance of 2x Thru is good up to roughly 40GHz. It helps to de-embed the fixture at high frequency. And the results of 1x DUT shows the good impedance control plus probe effect. Hence, the material of de-embedding looks acceptable.

Figure 4.7. Differential probe (D-probe).

The raw data point out that the differential probe has some variation due to the landing and minor manufacturing difference. The pick at around 2.4ns from the TDR impedance has 10 Ohm difference due to the landing position error. Therefore, the de-embedding results will have the same behavior as well.

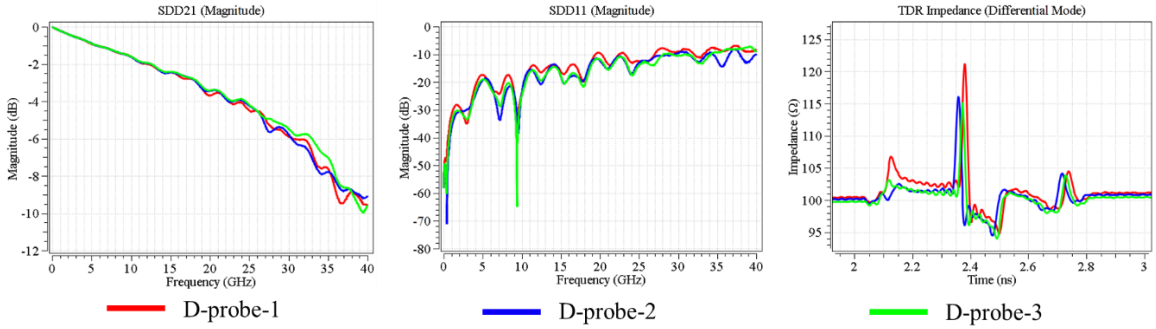

Figure 4.8. 1x DUT with different probes measurement results.

The de-embedding results, Figure 4.9, show the similar trend as the raw measurement results. From the $|S_{dd21}|$ and $|S_{dd11}|$, the three probes are located to the narrow range among the complete frequency band. The TDR impedance shows that the probe effects are captured successfully which agrees with the expectation. The huge bump at 2.4ps represent the touching point of probe. The inductance behavior is from the pair of probe tips. After the touching point, the previous transmission line is removed which means that the extracted S-parameters is only the probe itself.

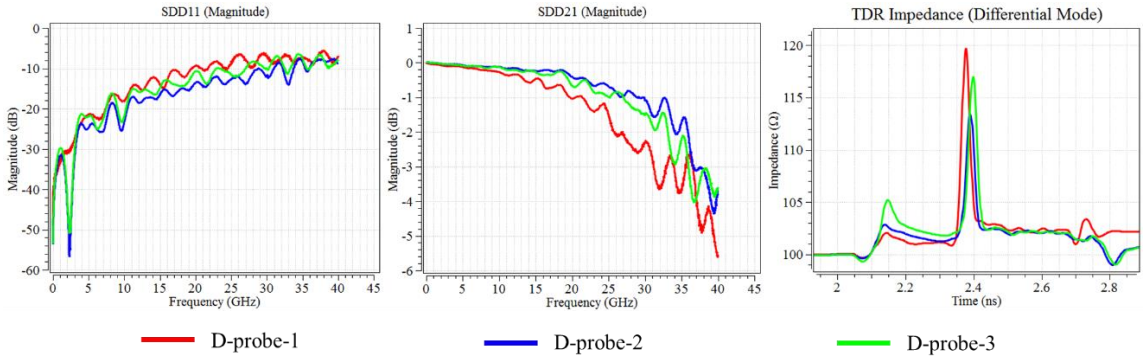

Figure 4.9. De-embedding results of different probes.

Another phenomenon should be pointed out from the results is that the variation of probe. The impedance of probe tip is from 112Ohm to 120Ohm. The variation of the probe makes the probe high accuracy model extraction very hard. Therefore, a general probe model would be more unify for the probe characterization.

4.5. FULL WAVE MODEL CONSTRUCTION

In this section a complete full wave model, Figure 4.10, is proposed to characterize the mentioned D-probe. The full wave model is built with a commercial full wave simulation tool with FDTD method. For getting a high accuracy model, several full wave model is designed based the physical dimensions of the probe and the designed testing board.

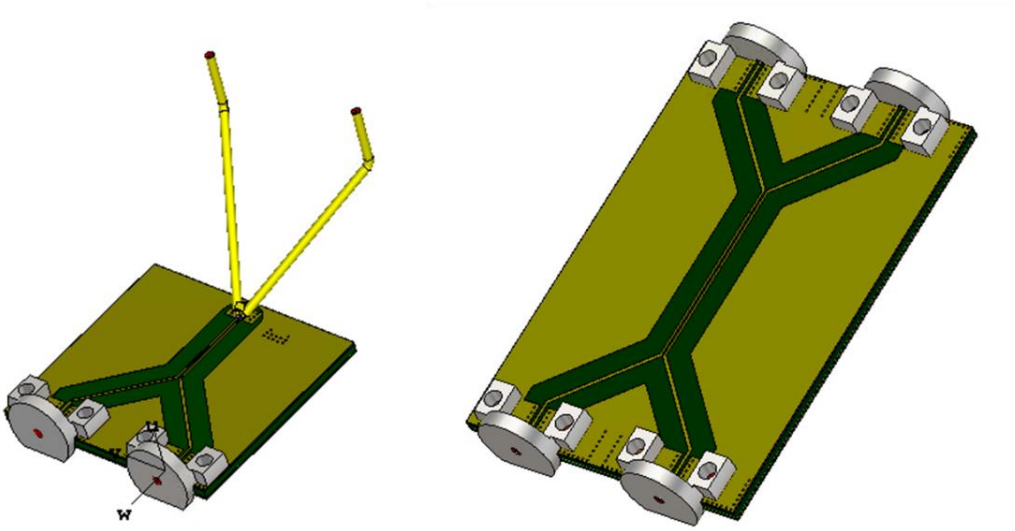

(a) (b)

Figure 4.10. (a) The full wave model of 1X and DUT (b) 2X thru model.

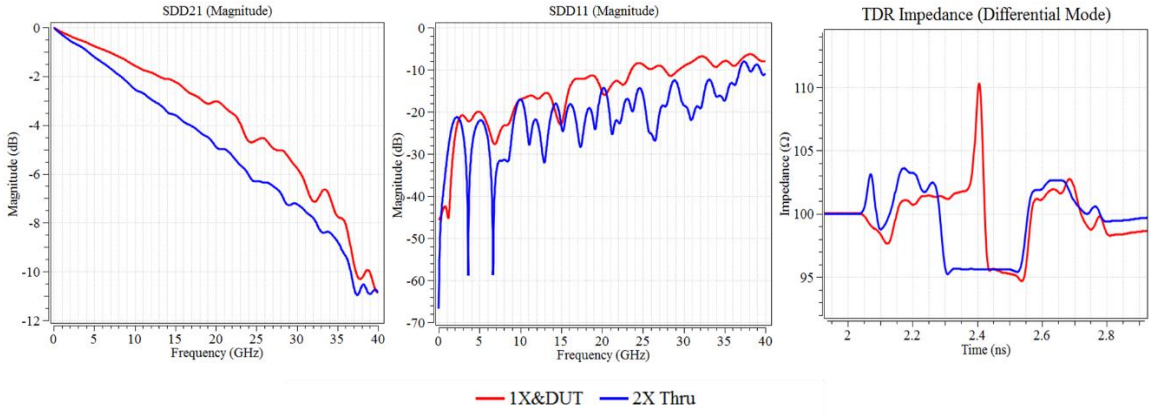

Figure 4.11. Full wave simulation raw data.

The two full models are shown in the Figure 4.11 and the raw data are shown below. Because the connector model isn't validated, and will be de-embedded. The raw data don't compare with the measurement data for avoiding misunderstanding. Applied the same de-embedding method, the de-embedded S-parameter of the full-model could be extracted. At the meantime, the cutting full wave model is created as well to prove the de-embedding method. The 1X&DUT model is cut. 60mil transmission line is remain to keep the output of the PCB is TEM mode.

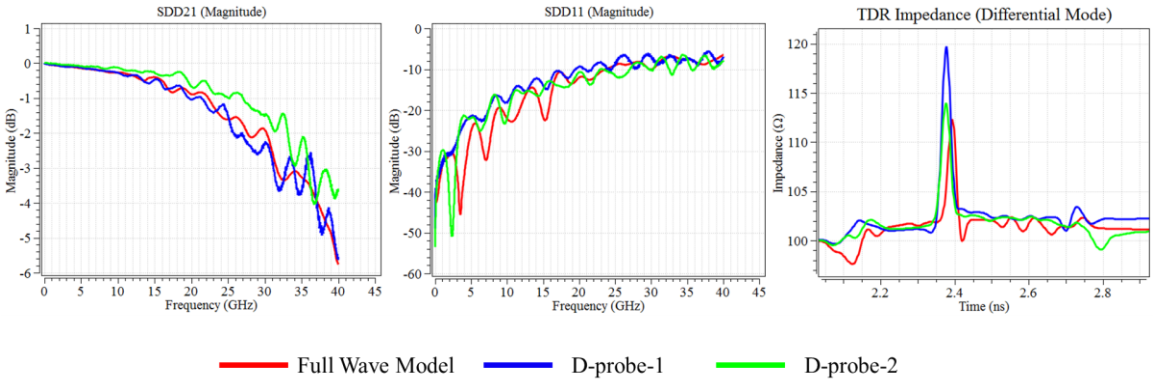

Figure 4.12. De-embedding results comparisons between the full wave model and the measurement de-embedding results.

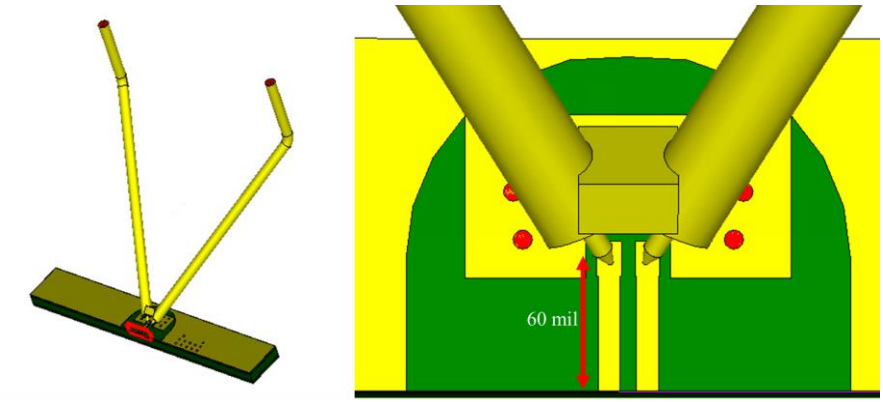

Figure 4.13. Full wave model of probe and the 60 mil microstrip.

From the Figure 4.12, the results shows that the measurement de-embedding results have same behavior as the raw data. The probes have different behavior at high frequency depends on the probe manufacturing. Therefore the probe model is designed to capture the major behavior of the probe as the Figure 4.13 shown. The $|S_{dd21}|$ and $|S_{dd11}|$ are at the same range comparing with the measurement results.

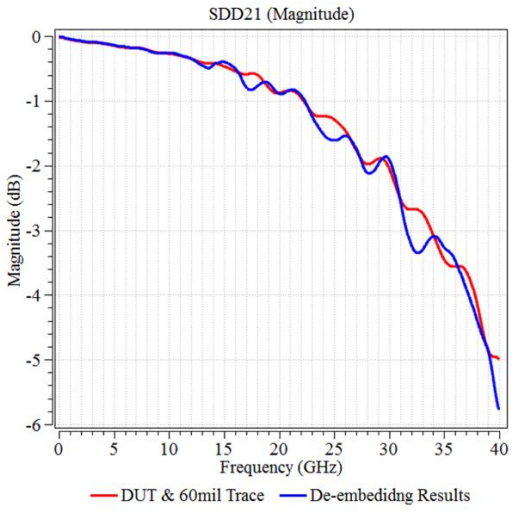

Figure 4.14. $|S_{dd21}|$ of probe and the only probe comparing with the de-embedding results.

For better understanding of the differential probe full wave model, a cutting model is built as well to demonstrate the de-embedding idea. The simulation results is shown in the Figure 4.14. The DUT with 60mil trace has more smooth $|S_{dd21}|$ comparing with the de-embedding results. The resason of the situation is from the impedance difference as show in the previous TDR comparison. Minor impedance mismatch of the DUT&1X and 2X thru lead to the not pure de-embedding.

Unfrindly ripple display after the probe effect. Regardless of the flatness of insertion loss, the two $|S_{dd21}|$ results have good agreement from the low frequency to high frequency which means the de-embedding method is working well and the real S-parameter of the DUT will be more smooth if the impedance mismatch could be overcomed.

4.6. CIRCUIT MODEL CONSTRUCTION

The circuit model [19] is propose to analysis the probe behavior in physical based on the current path as shown in the Figure 4.15.

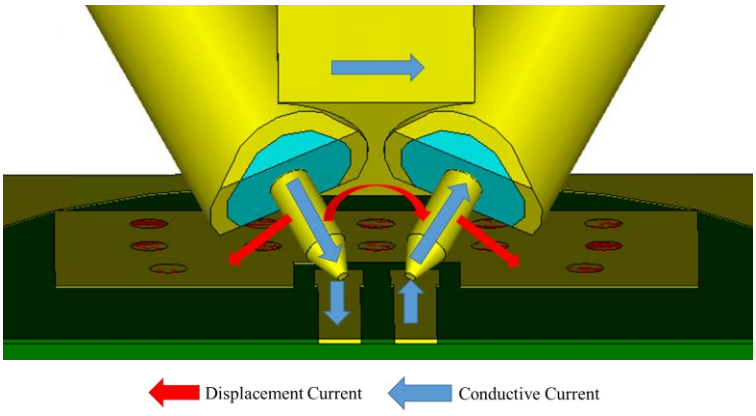

Figure 4.15. Current path analysis.

Because only differential signal run on the trace, the conductive current is from the one probe coaxial cable to the probe tip, then transmit to one of the differential microstrip. After going through all the conductor, the signal will return from the other microstrip then back to the probe. And the tips couple to the testing board as well which is treated as displacement current.

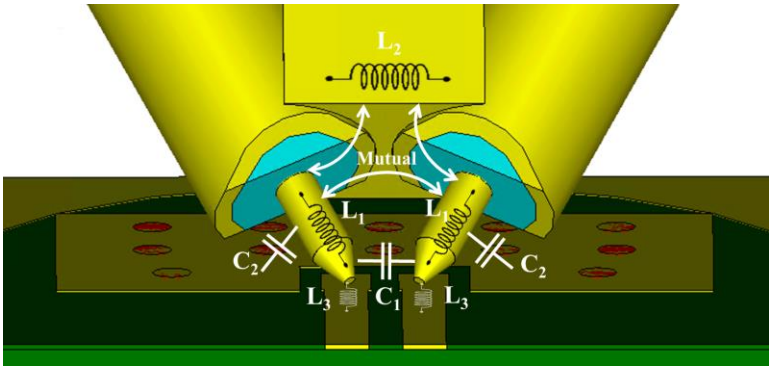

Figure 4.16. Circuit model of the probe tip.

Table 4.1. Lumped element.

C1	0.063pF	L1	0.49nH
C2	0.031pF	L2	0.23nH
Mutual L1&L1	0.081nH	L3	0.15nH
Mutual L1&L2	0.1nH		

Because the current distribution at the tip portion is complex and hard to be represent with sample transmission line. The circuit model is shown in the Figure 4.16. As the circuit diagram, the probe is represented with several lumped elements. The circuit

model is built in ADS (Advanced design system) to do the simulation. The circuit schematic is shown in the Figure 4.17.

The circuit model is composed with three portions, the connector and transmission line part, the lumped elements part which is probe tip and another a pair of microstrip which represents the extra 60mil differential pair. The each lumped elements are listed in the Table 4.1. The lumped element is tuned from the software which means the combination may not be unique.

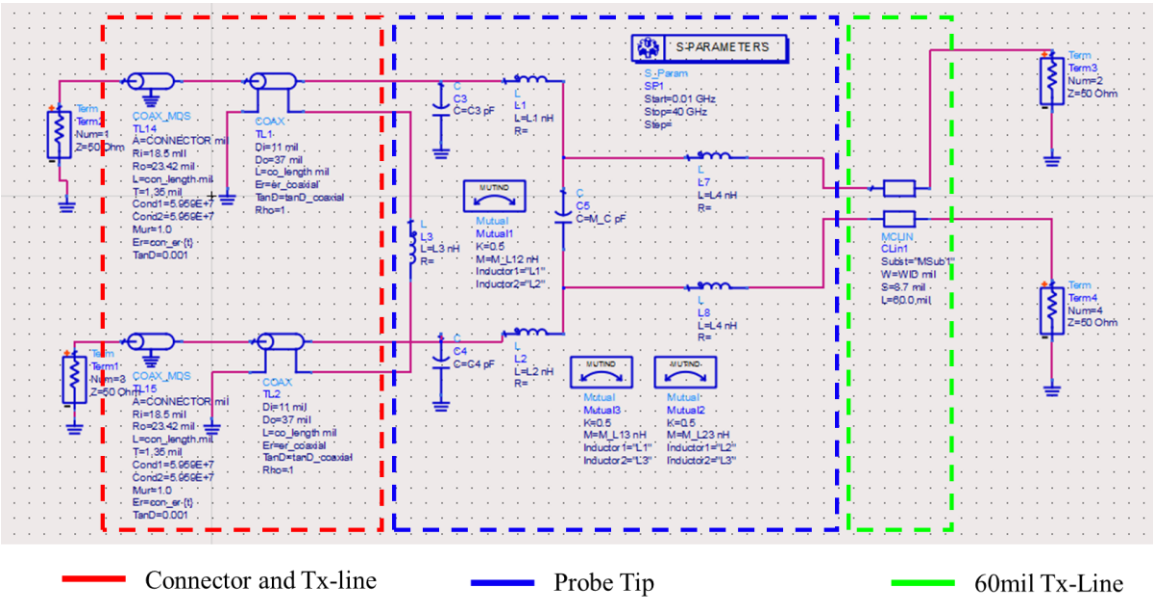

Figure 4.17. Circuit schematic in ADS.

As the results shown in the Figure 4.18, the TDR impedance shows that the circuit model reproduces the probe effects at the certain position. And the insertion loss and return loss are located in the range of the probe variation. But the circuit model is hard to

represent the wave of high frequency because of the lack of non-de-embedding information as previous discussed.

Therefore, the circuit model could be used to study the certain component behavior of the probe tip and has good relation in the TDR comparison. The frequency domain results is good to show the loss at different frequency range.

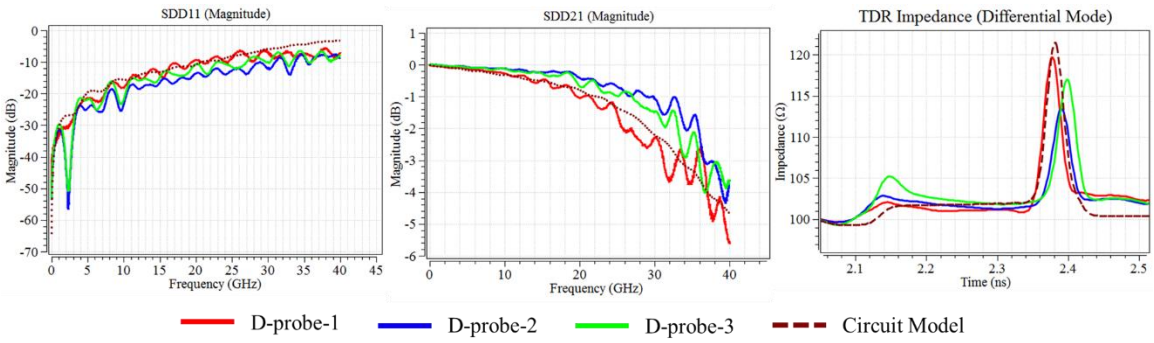

Figure 4.18. The results comparison between the circuit model and measurement.

4.7. SECTION SUMMARY

From the series of study of probe, the methodology of the probe S-parameter block extraction is workable. In this method, differential probe behavior could be captured easily even the probe manufacturing differences could be demonstrated. The full wave model is built to represent the probe behavior in the commercial 3D simulation tool and the circuit model is used to analysis the probe behavior based on the physical current path. Some improvable points are exposed as well. Because of the variation of the probes, the high accuracy of probe model is hardly to be extracted. The testing board could be remanufactured with better technics to overcome the mismatch problem. The method could be extend to more kinds of probe in the future.

5. CONCLUSION

In this thesis, two probing related topic are discussed. In the first topic, the unified probe landing pattern is designed based on 2 probe pitch and 3 kinds of differential probes. From the full wave simulation and testing board measurement, the landing pattern design is fixed and is proved with the good utilization. With the multiple probes supporting, the testing couple is designed for several purposes. Firstly, the accuracy probe de-embedding is applied by the design. Then the de-embedded results is used to characterize the PCB material which is confirmed by the connector measurement. In the second topic, the methodology of probe characterization, the probe is treated as a DUT instead of a fixture. With the high accuracy testing coupon design, the S-parameter block of block is extracted according to the design guideline. Then a general full wave model and a physical based circuit model are proposed and tested. The full wave model can be used as an accuracy reference to predict the probe behavior in the future probe application studying. And the circuit model is used to evaluate each component of the probe with the lumped element. In this way, the probe could be improved with the physical idea instead of the rule of thumb.

From the two topics, a serial of study is done related to the probe design and application design. Those experience is not only the recent study, but also can be extend to many new probe applications and also will be helpful in the real industrial for mass PCB production.

BIBLIOGRAPHY

[1] Z. Yan, J. Wang, W. Zhang, Y. Wang, and J. Fan, "A Miniature Ultrawideband Electric Field Probe Based on Coax-thru-hole Via Array for Near-Field Measurement," IEEE Trans. Instrum. Meas., vol. 66, no. 10, pp. 2762-2770, Oct. 2017.

[2] Z. Yan, J. Wang, W. Zhang, Y. Wang, and J. Fan, "A Simple Miniature Ultrawideband Magnetic Field Probe Design for Magnetic Near-Field Measurements," IEEE Trans. Antennas Propag., vol. 64, no. 12, pp. 5459-5465, Dec. 2016.

[3] X. Yan, Y. Wang, J. Zhou, and J. Fan, "A 20 GHz Landing Probe Design Based on Pogo-pins," in Proc. IEEE Symp. Electromagn. Compat. Signal Integrity, 2018, Long Beach, CA, USA, 2018, pp.

[4] Bichen Chen, Jiayi He, X.Ye, Shuai Jin, Jun Fan., "De-embedding Mode Conversion Characterization and Error Correction," Submitted to IEEE Trans. On Electromagnetic Compatibility, 2018

[5] Yuan Chen, Han Deng, Bichen Chen, Richard Zai, Jimmy Hsu, Xiaoning Ye, Jun Fan., "Signal-signal D-probe and Unified Launch Pads Designs," IEEE Electromagnetic Compatibility Magazine,2018, Jan.

[6] S. Jin, Bichen Chen, X. Fang, H. Gao and J. Fan., "Improved "Root-Omega" method for transmission-line based material property extraction for multilayer PCBs," IEEE Trans. On Electromagnetic Compatibility. Vol. 59, no. 4, pp1356-1367, March 2017.

[7] Bichen Chen, Xiaoning Ye, Bill Samaras, Jun Fan., "A novel de-embedding method suitable for transmission-line measurement," in 2015 Asia-Pacific Symposium on Electromagnetic Compatibility (APEMC). Symposium Best Student Paper finalist (http://www.apemc2015.org/BSPA.asp).

[8] Chunyu Wu, Bichen Chen, Tsiklauri Mikheil, Xiaoning Ye, Jun Fan., " Error Bounds Analysis of De-embedded Results in 2x Thru De-embedding Methods" in Electromagnetic Compatibility (EMC), 2017 IEEE International Symposium

[9] Qian Wang, Ketan Shringarpure, Bichen Chen, Jun Fan, Chulsoon Hwang, Siming Pan, Brice Achkir.,"Effectiveness analysis of de-embedding method for typical TSV pairs in a silicon interposer," in 2014 IEEE 23rd Conference on Electrical Performance of Electronic Packaging and Systems.

[10] J. Xu, L. Zhang, M. Sapozhnikov and J. Fan, "Application of Deep Learning for High-speed Differential Via TDR Impedance Fast Prediction," 2018 IEEE Symposium on Electromagnetic Compatibility, Signal Integrity and Power Integrity (EMC, SI & PI), Long Beach, CA, USA, 2018, pp. 645-649.

[11] L. Zhang et al., "EMI Coupling Paths and Mitigation in Optical Transceiver Modules," in IEEE Transactions on Electromagnetic Compatibility, vol. 59, no. 6, pp. 1848-1855, Dec. 2017.

[12] J. Li et al., "EMI coupling paths in silicon optical sub-assembly package," 2016 IEEE International Symposium on Electromagnetic Compatibility (EMC), Ottawa, ON, 2016, pp. 890-895.

[13] Q. Huang, J. Li, J. Zhou, W. Wu, Y. Qi and J. Fan, "De-embedding method to accurately measure high-frequency impedance of an O-shape spring contact," in Proc. of IEEE Int. Symp. Electromagn.Compat., 2014, pp. 600-603.

[14] Q. Huang, F. Zhang, T. Enomoto, J. Maeshima, K. Araki and C. Hwang, "Physics-based dipole moment source reconstruction for RFI on a practical cellphone", IEEE Trans. Electromagn. Compat., vol. 59, no. 6, pp. 1693-1700, Dec. 2017.

[15] S. Jin, D. Liu, B. Chen, R. Brooks, K. Qiu, J. Lim, and J. Fan, “Analytical Equivalent Circuit Modeling for BGA in High-Speed Package IEEE Transactions on Electromagnetic Compatibility. Vol. 60, pp 68-76, Feb 2018.

[16] Shuai Jin, X. Fang, B. Chen, H. Gao, X. Ye and J. Fan, “Validating the transmission-line based material property extraction procedure including surface roughness for multilayer PCBs using simulations,” in Proc. IEEE Int. Symp. EMC, Ottawa, CN, July. 25-29, 2016.

[17] Shuai Jin, J. Zhang, J. Lim, K. Qiu, R. Brooks, and J. Fan, “Analytical Equivalent Circuit Modeling for Multiple Core Vias in a High-Speed Package,” in Proc. IEEE Int. Symp. EMC, Ottawa, CN, July. 25-29, 2016.

[18] B. Chen, M. Tsiklauri, C. Wu, Shuai Jin, J. Fan, X. Ye and B. Samaras, “Analytical and numerical sensitivity analyses of fixtures de-embedding,” in Proc. IEEE Int. Symp. EMC, Ottawa, CN, July. 25-29, 2016

[19] Y. S. Cao, L. Jiang and A. E. Ruehli, “An equivalent circuit model for graphene-based terahertz antenna using the PEEC method,” IEEE Trans. Antenna Propag., vol. 64, no. 4, pp. 1385–1393, Apr. 2016.

[20] Z. Yan, J. Wang, W. Zhang, Y. Wang and J. Fan, "A Simple Miniature Ultrawideband Magnetic Field Probe Design for Magnetic Near-Field Measurements," in IEEE Transactions on Antennas and Propagation, vol. 64, no. 12, pp. 5459-5465, Dec. 2016.

[21] Z. Yan, J. Wang, W. Zhang, Y. Wang and J. Fan, "A Miniature Ultrawideband Electric Field Probe Based on Coax-Thru-Hole via Array for Near-Field Measurement," in IEEE Transactions on Instrumentation and Measurement, vol. 66, no. 10, pp. 2762-2770, Oct. 2017.

VITA

Han Deng received the B.E. degree in Electrical Engineering from the University of Electronic Science and Technology of China, Chengdu, China, in 2014. He joined the Electromagnetic Compatibility Laboratory in 2016. He received the Master of Science in Electrical Engineering from Missouri S&T in May 2019.

His research interests included signal integrity, probe design, high speed PCB design.